Published in final edited form as:
Nat Neurosci. 2020 January ; 23(1): 21–31. doi:10.1038/s41593-019-0541-x.

α-Synuclein Strains Target Distinct Brain Regions and Cell Types

Angus Lau[#1,2], **Raphaella W.L. So**[#1,2], **Heather H.C. Lau**[1,2], **Jason C. Sang**[3], **Alejandro Ruiz-Riquelme**[1,^], **Shelaine C. Fleck**[4,5], **Erica Stuart**[1], **Sindhu Menon**[1], **Naomi P. Visanji**[6,7], **Georg Meisl**[3], **Rania Faidi**[1], **Maria M. Marano**[1,8], **Cian Schmitt-Ulms**[1], **Zhilan Wang**[1], **Paul E. Fraser**[1,9], **Anurag Tandon**[1,8], **Bradley T. Hyman**[10,11,12], **Holger Wille**[4,5], **Martin Ingelsson**[13], **David Klenerman**[3], **Joel C. Watts**[1,2,*]

[1]Tanz Centre for Research in Neurodegenerative Diseases, University of Toronto, Toronto, Ontario, Canada

[2]Department of Biochemistry, University of Toronto, Toronto, Ontario, Canada

[3]Department of Chemistry, University of Cambridge, Cambridge, United Kingdom

[4]Centre for Prions and Protein Folding Diseases, University of Alberta, Edmonton, Alberta, Canada

[5]Department of Biochemistry, University of Alberta, Edmonton, Alberta, Canada

[6]Morton and Gloria Shulman Movement Disorders Centre, Toronto Western Hospital, Toronto, Ontario, Canada

[7]Edmond J. Safra Program in Parkinson's Disease, Toronto Western Hospital, Toronto, Ontario, Canada

[8]Department of Medicine, University of Toronto, Toronto, Ontario, Canada

[9]Department of Medical Biophysics, University of Toronto, Toronto, Ontario, Canada

[10]Department of Neurology, Massachusetts General Hospital, Charlestown, Massachusetts, USA

[11]Department of Radiology, Massachusetts General Hospital, Charlestown, Massachusetts, USA

[12]Neuroscience Program, Harvard Medical School, Boston, Massachusetts, USA

[*]To whom correspondence should be addressed at: Krembil Discovery Tower, Rm. 4KD481, 60 Leonard Ave., Toronto, ON, Canada, M5T 0S8; Tel: (416) 507-6891; Fax: (416) 603-6435; joel.watts@utoronto.ca.
[^]Present address: German Center for Neurodegenerative Diseases (DZNE), Tübingen, Germany

Data Availability Statement

The data that support the findings of this study are available from the corresponding author upon request.

Author Contributions

Designed the experiments: DK and JCW; Conducted the experiments: AL, RWLS, HHCL, JCS, AR-R, SCF, ES, SM, NPV, RF, MMM, CSU, and ZW. Analyzed and interpreted the data: AL, GM, PEF, AT, BTH, HW, MI, DK, and JCW. Wrote the manuscript: JCW. All authors edited and approved the manuscript.

Competing Interests Statement

The authors declare no competing interests.

Europe PMC Funders Author Manuscripts

[13]Department of Public Health and Caring Sciences / Geriatrics, Uppsala University, Uppsala, Sweden

[#] These authors contributed equally to this work.

Europe PMC Funders Author Manuscripts

Abstract

The clinical and pathological differences between synucleinopathies such as Parkinson's disease and multiple system atrophy have been postulated to stem from unique strains of α-synuclein aggregates, akin to what occurs in prion diseases. Here, we demonstrate that inoculation of transgenic mice with different strains of recombinant or brain-derived α-synuclein aggregates produces clinically and pathologically distinct diseases. Strain-specific differences were observed in the signs of neurological illness, time to disease onset, morphology of cerebral α-synuclein deposits, and the conformational properties of the induced aggregates. Moreover, different strains targeted distinct cellular populations and cell types within the brain, recapitulating the selective targeting observed between human synucleinopathies. Strain-specific clinical, pathological, and biochemical differences were faithfully maintained upon serial passaging, implying that α-synuclein propagates via prion-like conformational templating. Thus, pathogenic α-synuclein exhibits key hallmarks of prion strains, providing evidence that disease heterogeneity among the synucleinopathies is caused by distinct α-synuclein strains.

Parkinson's disease (PD) and related diseases, including dementia with Lewy bodies (DLB) and multiple system atrophy (MSA), are progressive neurodegenerative disorders. The brains of PD, DLB, and MSA patients contain intracellular inclusions composed of aggregated α-synuclein (α-syn). Thus, these diseases are commonly referred to as α-synucleinopathies, or simply synucleinopathies[1]. α-Syn is a 140-amino acid cytoplasmic protein that is found within presynaptic nerve terminals and is involved in the assembly of SNARE complexes[2]. In disease, α-syn polymerizes into insoluble β-sheet-rich protein aggregates that become phosphorylated at residue Ser129 and deposit within the central nervous system[3, 4]. α-Syn is believed to play a central pathogenic role in the synucleinopathies since mutation of the gene encoding α-syn causes early-onset PD[5].

There is mounting evidence that α-syn becomes "prion-like" during disease, leading to a progressive cell-to-cell spreading of protein aggregates within the brain[6]. Prions are self-propagating protein aggregates that cause neurodegenerative disorders such as Creutzfeldt-Jakob disease in humans and scrapie in sheep. Prion replication and spreading is thought to occur via a template-directed refolding mechanism, in which aggregated prion protein (PrP) catalyzes the conformational conversion of properly-folded PrP into additional copies of the misfolded form[7]. Similar to the experimental transmission of prion disease, injection of mice with pre-formed α-syn aggregates induces the aggregation and deposition of α-syn within the brain and, in some instances, accelerates the onset of neurological illness[8–13]. The prion-like behavior of α-syn aggregates provides a potential molecular explanation for the progressive nature of PD and related synucleinopathies.

The synucleinopathies are clinically and pathologically heterogeneous, with prominent disease-specific differences in clinical presentation, rate of disease progression, and the brain regions and cell types vulnerable to α-syn deposition and cellular death[14, 15]. Different types

of cerebral α-syn inclusions are observed among the synucleinopathies: the pathological hallmark of PD and DLB is the presence of Lewy bodies (LBs) and Lewy neurites within neurons, whereas MSA is characterized by cytoplasmic inclusions within oligodendrocytes. One potential explanation for this phenotypic diversity is the presence of different strains of α-syn aggregates, similar to what occurs in prion diseases. Prion strains are different types of prions that possess distinct biochemical and pathological properties[16]. Strain-specific attributes are encoded by unique conformational states of PrP aggregates[17]. Prion strains can be differentiated by their incubation periods upon inoculation into animals and the resultant clinical signs of neurological illness, by the location and morphology of prion aggregates within the brain, and by their conformational properties. A key feature of prion strains is that their biological properties are maintained upon serial transmission due to template-directed misfolding.

Several recent studies have provided evidence that α-syn can exhibit strain-like behavior *in vitro* and upon inoculation into rodents. For instance, recombinant α-syn can be polymerized into distinct aggregated states that exhibit differential toxicities when applied to cultured cells, demonstrate distinct abilities to promote tau inclusions in neurons, and display variable capacities to spread and induce pathology when injected into rodents[18–20]. Furthermore, different synucleinopathy samples exhibit distinct seeding capacities *in vitro* and *in vivo*, with MSA-derived α-syn aggregates being more potent inducers of α-syn pathology than PD-derived aggregates[21–24]. MSA brain extracts can also induce distinct α-syn pathologies when injected into different lines of transgenic mice[25]. While these results are consistent with the existence of α-syn strains, whether distinct conformational states of α-syn aggregates exhibit all the salient properties of prion strains when propagated in animals, including the ability to initiate truly distinct, serially transmissible synucleinopathies in the same host remains unknown.

Here, we demonstrate that different strains of recombinant or brain-derived α-syn aggregates produce unique motor, pathological, and biochemical phenotypes upon propagation in TgM83 transgenic mice. Most notably, different α-syn strains target distinct brain regions and cell types within the inoculated mice, recapitulating the selective targeting observed between different human synucleinopathies. Strain-specific phenotypic differences are maintained upon serial transmission, indicating that α-syn aggregate strains propagate via a prion-like templating mechanism and thus behave similarly to prion strains.

Results

Generation of recombinant α-syn fibril strains

We hypothesized that unique conformational states of α-syn aggregates ("α-syn strains") would produce distinct phenotypes when propagated in the TgM83 synucleinopathy mouse model, which over-expresses α-syn containing the disease-causing A53T mutation[26]. Based on the published success of generating distinct recombinant α-syn strains by varying buffer conditions during fibril formation[19, 20], we initially searched for conditions that produced A53T-mutant human α-syn fibrils with divergent conformational properties. We focused on fibrils since they appear to be more potent inducers of PD-like neuropathology than α-syn oligomers upon injection into mice[20, 27]. Polymerization of recombinant α-syn in either the

presence or absence of 100 mM NaCl was found to generate conformationally distinct aggregates, which we termed Salt ("S") and No Salt ("NS") fibrils (Fig. 1a). In real-time Thioflavin T (ThT) fluorescence aggregation assays, the lag phase for S fibril formation was significantly shorter than for NS fibrils (Fig. 1b). Interestingly, NS fibrils consistently bound much less ThT than S fibrils, possibly indicating structural differences between the two types of fibrils (Fig. 1c). Indeed, NS fibrils were significantly longer than S fibrils (Fig. 1d) and distinct banding patterns were obtained following digestion of the two fibril types with proteinase K (PK) (Fig. 1e). Moreover, the fluorescence emission spectra obtained following binding of the conformation-sensitive dye curcumin[28] to S and NS fibrils were markedly different (Fig. 1f, Extended Data 1). Finally, using a conformational stability assay (CSA) that measures the differential abilities of protein aggregate strains to resist denaturation by guanidine hydrochloride (GdnHCl), we found that S fibrils were significantly less stable than NS fibrils (Fig. 1g, h). Taken together, these results demonstrate that the S and NS fibril preparations contain conformationally distinct species of α-syn aggregates.

Next, we assessed whether S and NS fibrils could seed the formation of distinct α-syn aggregates in cultured cells. Using liposome-mediated transduction, various forms of α-syn were introduced into HEK293 cells that stably express human A53T-mutant α-syn fused at its C-terminus with yellow fluorescent protein (YFP)[29] (Extended Data 2). When cells were treated with monomeric (non-polymerized) recombinant A53T-mutant α-syn, only diffuse cytoplasmic fluorescence was observed. In contrast, the transduction of either S or NS fibrils resulted in the production of fluorescent foci, which are indicative of the formation of α-syn(A53T)-YFP aggregates. The morphologies of the resultant aggregates differed between the fibril strains: cells exposed to S fibrils developed globular aggregates whereas cells treated with NS fibrils developed thread-like aggregates (Extended Data 2).

Propagation of α-syn strains in TgM83 mice

When injected into mice, prion strains produce distinct disease phenotypes that are faithfully maintained over serial passaging. To assess whether the same is true of α-syn strains *in vivo*, we performed propagation studies in hemizygous TgM83 mice (Fig. 2a), which can develop a synucleinopathy following inoculation with pre-formed α-syn aggregate seeds[9, 10]. Hemizygous TgM83 mice were used since they remain healthy for up to at least 20 months of age (Table 1)[10], whereas homozygous mice ($M83^{+/+}$) develop spontaneous signs of neurological illness beginning at around 8 months of age[26]. To determine whether disease phenotypes can be faithfully maintained over multiple passages, brain extracts from previously inoculated mice were used as inocula for serial transmission experiments (Fig. 2a).

Equal amounts (1 μg) of S and NS fibril preparations were intracerebrally inoculated into weanling TgM83 mice. As negative controls, we injected mice with either phosphate-buffered saline (PBS) or non-polymerized monomeric A53T-mutant α-syn. None of the control-inoculated mice developed signs of neurological illness for up to 18 months post-inoculation (Table 1, Fig. 2b). While both groups of fibril-injected animals developed signs of neurological illness consistent with a synucleinopathy, the disease incubation periods were markedly different. Mice injected with NS fibrils took longer to develop disease than

mice injected with S fibrils, and the distinct disease kinetics were maintained over serial passaging (Table 1, Fig. 2b, c). Strikingly, the clinical signs of neurological illness differed in the fibril-inoculated mice (Supplementary Videos 1-6). Mice injected with S fibrils presented with partial or complete hind-limb paralysis accompanied by bradykinesia whereas NS fibril-injected mice presented with weight loss, mild kyphosis, and a unique hind-limb shaking phenotype. The divergent clinical profiles were maintained upon second and third passage of the S and NS fibril-derived strains.

To search for a molecular explanation for the incubation period differences, we employed a single-molecule fluorescence approach to study the relative multiplication rates of S and NS fibrils. In this assay, monomeric A53T-mutant α-syn is seeded with either S or NS fibrils, and then fibril length is measured as a function of time by ThT staining and total internal reflection fluorescence microscopy[30]. Using this approach, the time taken for the number of aggregates to double can be calculated as a function of the rate constants for fibril elongation and fragmentation (Extended Data 3). In accordance with the *in vivo* propagation results, these experiments indicated that NS fibrils exhibit an increased doubling time compared to S fibrils, which can be attributed almost exclusively to their decreased rate of fragmentation (Extended Data 3, Supplementary Table 1).

To determine if strain-like behavior also occurs with α-syn aggregates generated in a more physiological environment, we performed transmission studies in TgM83 mice with putative brain-derived strains of α-syn aggregates (Fig. 2a). It has previously been shown that brain extracts from MSA patients and sick M83$^{+/+}$ mice produce distinct disease kinetics when injected into TgM83 mice[10, 11]. In agreement with these results, disease incubation periods following inoculation with brain extract from an MSA patient were significantly shorter than for TgM83 mice inoculated with brain extract from a spontaneously sick M83$^{+/+}$ mouse (Table 1, Fig. 2d, e). The incubation period difference was also observed upon second passage of the two brain-derived strains. Moreover, the clinical signs of neurological illness were distinct in MSA- and M83$^{+/+}$-inoculated TgM83 mice and were maintained following second passage. Hind-limb paralysis and bradykinesia predominated in MSA-challenged mice, similar to the phenotype observed in mice inoculated with S fibrils, whereas hind-limb shaking, weight loss, and mild kyphosis were observed in M83$^{+/+}$-inoculated mice, similar to the phenotype induced by inoculation with NS fibrils (Supplementary Videos 7-8).

Detergent-insoluble α-syn species were detected in brain homogenates from all mice examined, including asymptomatic buffer-inoculated animals (Fig. 2f), likely due to the over-expression of mutant α-syn in the TgM83 line. However, only the brains of mice injected with α-syn fibrils, M83$^{+/+}$ extract, or MSA extract contained detergent-insoluble α-syn species that were partially resistant to digestion with the protease thermolysin (TL). Moreover, insoluble α-syn phosphorylated at Ser129 (PSyn), a marker for disease-associated α-syn species[3], was only detected in brain extracts from the animals injected with samples containing α-syn aggregates (Fig. 2f). Identical results were obtained with brain samples from the serial transmission of the fibril-derived and brain extract-derived strains (Extended Data 4). Since TgM83 mice express both A53T-mutant human α-syn and endogenous murine α-syn, we checked whether the induced α-syn aggregates were composed of human α-syn, mouse α-syn, or a mixture of both. TL-resistant α-syn species in the inoculated

TgM83 mice were detectable using an antibody specific to human α-syn but not with an antibody specific for mouse α-syn, indicating that aggregates are composed exclusively of human α-syn (Extended Data 4). By immunohistochemistry, PSyn deposits were observed in the brains of all TgM83 mice inoculated with α-syn fibrils, $M83^{+/+}$ extract, or MSA extract, but not in the brains of mice injected with PBS or monomeric α-syn (Extended Data 5). Together, these results confirm that TgM83 mice develop a synucleinopathy following injection with various α-syn strains.

α-Syn strains produce distinct synucleinopathies in TgM83 mice

The distribution of PSyn deposits within the brain differed in mice injected with either S or NS fibrils, and these distinct signatures were maintained upon serial passaging (Fig. 3a). Both groups of inoculated mice exhibited prominent PSyn pathology in the midbrain, brainstem, and hypothalamus (Fig. 3a, Extended Data 5). However, only mice injected with NS fibrils displayed PSyn deposition in the hippocampus and olfactory bulb, and NS fibril-injected mice had significantly higher levels of PSyn pathology in the cortex than mice inoculated with S fibrils (Fig. 3a, b). Similar to what was observed in mice injected with fibril-derived strains, the neuroanatomical distributions of PSyn pathology in TgM83 mice injected with MSA or $M83^{+/+}$ extract were also distinct and stably maintained upon serial passaging (Fig. 3c). Higher levels of cortical PSyn deposition were observed in the $M83^{+/+}$-injected animals, and hippocampal as well as olfactory bulb PSyn pathology was exclusively present in mice inoculated with $M83^{+/+}$ extract (Fig. 3c, d). Extensive PSyn deposition within the midbrain, brainstem, and hypothalamus was present in mice injected with either MSA or $M83^{+/+}$ (Fig. 3c, Extended Data 5). In general, mice injected with either the NS fibril- or $M83^{+/+}$-derived strains exhibited more widespread deposition of PSyn than mice injected with the S fibril- or MSA-derived strains.

In addition to the region-specific differences in PSyn deposition displayed by the various α-syn strains, the cellular tropism of the aggregates was also distinct. In TgM83 mice injected with S fibrils, PSyn pathology was exclusively observed within neurons (Extended Data 5). While mice injected with NS fibrils also exhibited neuronal PSyn deposition, PSyn staining was additionally observed within astrocytes (Fig. 4a, b). Astrocytic PSyn pathology was observed across all three passages of the NS fibril-derived strain. TgM83 mice injected with $M83^{+/+}$ extract also displayed PSyn pathology within astrocytes (Fig. 4a, b), whereas the PSyn deposits in MSA-injected mice were only found in neurons (Extended Data 5). In mice injected with either the NS fibril- or $M83^{+/+}$-derived strains, cellular co-localization was observed between PSyn staining and the astrocyte-specific marker glial fibrillary acidic protein (GFAP), confirming that the PSyn deposits were present within astrocytes (Fig. 4c).

In regions of the brain targeted by both the S and NS fibril strains, such as the midbrain and hypothalamus, the morphology of the induced α-syn deposits differed substantially. Ring-like PSyn deposits that filled the entire cell body surrounding the nucleus were found within neurons of mice inoculated with S fibrils (Fig. 5a, b). These inclusions were morphologically similar to the neuronal cytoplasmic inclusions found in the hippocampus of patients with atypical MSA[31]. In contrast, single large and dense LB-like PSyn deposits were found within the cytoplasm of neurons from mice inoculated with NS fibrils (Fig. 5a,

b). These distinct aggregate morphologies could also be visualized using antibodies to total α-syn as well as to p62/SQSTM1, indicating that both types of deposits were targeted for autophagy (Extended Data 6). Mice injected with MSA extract exhibited ring-like PSyn deposits whereas mice injected with $M83^{+/+}$ extract displayed LB-like PSyn deposits, mirroring the pathological differences in mice injected with S or NS fibrils (Fig. 5a, b). The distinct morphologies of PSyn deposits were maintained following serial passaging in TgM83 mice. Thus, much like prion strains, α-syn strains can target distinct regions and cell types within the brain and induce the formation of aggregates with distinct morphologies.

Biochemical analyses of the α-syn aggregates in the brains of mice inoculated with the various α-syn strains revealed conformational differences. The banding pattern of PK-resistant α-syn species in mice injected with S fibrils was slightly different from that in mice injected with NS fibrils. While both groups of mice possessed a band at ~9 kDa, mice injected with S fibrils exhibited an additional band at ~10 kDa whereas mice injected with NS fibrils displayed a prominent additional lower band at ~7 kDa (Fig. 5c). The distinct PK digestion signatures were maintained upon serial passaging, but only partially overlapped with the pattern generated by digestion of the original fibrils (Extended Data 7). Similar differences in PK-resistant α-syn banding patterns were observed between MSA- and $M83^{+/+}$-injected mice (Fig. 5c). As assessed by the CSA, the aggregates present in S fibril-injected mice were significantly less stable upon exposure to GdnHCl than those in NS fibril-inoculated animals, and this difference in conformational stability was preserved upon serial propagation (Fig. 5d, e, Extended Data 8). Across two passages, the α-syn aggregates in TgM83 mice injected with MSA extract were also more susceptible to GdnHCl denaturation than those in mice inoculated with $M83^{+/+}$ extract (Extended Data 8), reminiscent of the differences observed between animals inoculated with the S or NS fibril-derived strains.

Not all recombinant α-syn strains produce distinct synucleinopathies in TgM83 mice

Having established that the S and NS strains of recombinant α-syn aggregates can produce distinct synucleinopathies, we wondered whether additional strains could be propagated in TgM83 mice. To this end, we generated fibrils from wild-type (WT) or A53T-mutant recombinant human α-syn using either a continuous shaking protocol or by intermittent sonication using protein misfolding cyclic amplification (PMCA). Consistent with previous results[32], recombinant α-syn aggregated rapidly during the PMCA procedure and produced very short fibrils (Fig. 6a, Extended Data 9). Following PK digestion, we found that the PMCA fibrils made from WT α-syn exhibited a banding pattern that was distinct from both the S and NS fibrils (Fig. 6b, Extended Data 9). Inoculation of TgM83 mice with PMCA fibrils composed of WT α-syn produced a synucleinopathy characterized by neurological symptoms similar to those observed in mice inoculated with either S fibrils or MSA extract, whereas mice injected with monomeric WT α-syn remained asymptomatic (Table 1, Extended Data 9, Supplementary Videos 9-10). Upon serial passage, the survival curve and incubation periods observed for the PMCA fibril strain were very similar to those observed upon passage of the S fibril-derived strain (Fig. 6c, d). Moreover, the brain regions targeted, the morphology of the cerebral PSyn deposits, and the conformational properties of the induced α-syn aggregates in PMCA fibril-injected TgM83 mice were very similar to those

in mice injected with the S fibril-derived strain (Fig. 6e-g, Extended Data 9). Thus, not all conformationally-distinct recombinant α-syn fibril preparations produce unique disease phenotypes when propagated in TgM83 mice.

Characterization of α-syn strains from synucleinopathy patients

Finally, we looked for strain-specific differences in α-syn aggregates present in brain homogenates from synucleinopathy patients. As judged by the CSA, the α-syn aggregates present in MSA patients were significantly less stable than those present in the brains of either DLB patients or Alzheimer's disease (AD) patients with concomitant deposition of α-syn[33] (Fig. 7a, b). As described above and in previous papers[10, 11], brain extracts from MSA patients transmit disease to TgM83 mice with a mean incubation period of ~200 days (Table 1). In contrast, brain extract from a DLB patient or an AD patient, both of which contained TL-resistant α-syn (Extended Data 10), failed to produce neurological illness in TgM83 mice for up to 18 months post-inoculation (Table 1). Moreover, there was no evidence for increased amounts of PSyn deposition in the brains of DLB- or AD-inoculated mice compared to mice injected with PBS (Extended Data 10). Therefore, the investigated DLB and AD brains seem to contain strains of α-syn aggregates that do not propagate efficiently in TgM83 mice.

Discussion

Here, we show that α-syn strains, either originating from recombinant fibrils or derived from certain types of synucleinopathy brains, cause distinct synucleinopathies and exhibit key features reminiscent of prion strains, including 1) variable disease incubation periods upon propagation in a mouse model; 2) unique clinical signs of neurological illness; 3) different neuropathological profiles, including variability in regional and cellular vulnerability to protein deposition; 4) distinct conformations of protein aggregates; and 5) the ability to be serially transmitted. Therefore, the existence of α-syn strains provides a plausible explanation for the divergent clinical and pathological disease phenotypes observed among and within the human synucleinopathies. Moreover, these results add to a growing body of literature demonstrating that protein aggregates associated with neurodegenerative diseases, such as those made up of Aβ and tau, can exhibit strain-like behavior by specifying distinct phenotypes when propagated in animal models[28, 34–38]. The undeniable similarities between α-syn strains and prion strains provide further evidence of the prion-like properties of α-syn aggregates, although it is possible that the specific infectivity of α-syn strains is much lower than that of authentic prion strains.

The different salt concentrations we utilized to generate the S and NS fibril strains are unlikely to explain the genesis of distinct α-syn strains *in vivo*, where the cell type in which an aggregate initially forms likely plays a major role in defining its propagation behavior[22]. Nonetheless, the synucleinopathies induced by inoculation of TgM83 mice with S or NS fibrils were markedly different, indicating that conformational differences within α-syn aggregates underlie the phenotypic heterogeneity. For our *in vivo* propagation studies, we used hemizygous TgM83 mice, which express A53T-mutant α-syn at 3-4 times the levels found in the brains of non-transgenic mice[26]. We could not detect any mouse α-syn within

the induced α-syn aggregates in the inoculated mice, suggesting that high sequence homology between substrate and seed is required for efficient α-syn strain propagation. This is in agreement with a study that found that ablation of the mouse α-syn gene in TgM83 mice had no effect on the kinetics of disease following inoculation with MSA[11]. However, others have found that elimination of mouse α-syn promotes the aggregation of human α-syn[39]. While α-syn overexpression in the TgM83 line facilitated our results by allowing observable disease phenotypes (particularly those encoded by the NS fibril and $M83^{+/+}$ strains) to occur within the normal lifespan of the mouse, its role, if any, in modulating the strain-like behavior of α-syn aggregates remains to be determined. However, it should be noted that α-syn aggregates can be readily propagated in non-transgenic mice[12], and α-syn strain-specific effects on tau aggregation can be recapitulated in mice that do not overexpress α-syn[18].

Different α-syn strains selectively targeted different brain regions and cell types in TgM83 mice, reminiscent of the selective targeting observed in the synucleinopathies[15]. There are several potential explanations for this phenomenon. Multiple putative cell-surface α-syn receptors have been identified that are capable of facilitating import of α-syn aggregates into the cell and the initiation of downstream signaling pathways[40–42]. It is conceivable that these receptors could be differentially expressed between cellular populations within the brain and exhibit variable binding affinities for distinct α-syn strains, leading to different rates of aggregate internalization and subsequent propagation. It has also been speculated that cellular differences in α-syn expression level may contribute to selective aggregate vulnerability[43], and it is possible that different α-syn strains may propagate with differing efficiencies dependent on the level of α-syn substrate available. Alternatively, there may be cell- and strain-specific differences in rates of α-syn aggregate degradation. Interestingly, we found that inoculation with NS fibrils produced cerebral α-syn deposits in TgM83 mice that were more reminiscent of the LBs found in the brains of PD and DLB patients than the deposits obtained upon inoculation with other types of pre-formed α-syn fibrils[9]. Moreover, these mice selectively developed α-syn inclusions within the olfactory bulb and cortex, and exhibited α-syn pathology within astrocytes, similar to what occurs in PD and DLB patients[44, 45]. This suggests that TgM83 mice injected with the NS fibril-derived strain may be a valuable model for investigating PD- and/or DLB-related disease mechanisms and assessing candidate therapeutics.

We found that α-syn strains with lower conformational stability, such as those derived from S fibrils or MSA patient brain extract, propagated more rapidly in TgM83 mice than strains with intermediate conformational stability, such as those originating from NS fibrils or $M83^{+/+}$ brain extract. Moreover, highly stable α-syn strains, such as those present in the brains of the DLB and AD cases analyzed, failed to cause overt disease when injected into TgM83 mice. This inverse relationship between conformational stability and propagation rate has previously been documented in prion disease[46]. The molecular mechanism underpinning this observation remains to be determined but could be related to strain-specific differences in rates of aggregate fragmentation and cell-to-cell propagation as well as susceptibility to cellular degradation. It is easy to conceptualize how smaller, less stable protein aggregates may be able to spread between neighboring cells more efficiently than bulkier, more stable protein aggregates. Indeed, we found that S fibrils were shorter,

Europe PMC Funders Author Manuscripts

fragmented at a higher rate, and exhibited faster doubling times than NS fibrils. The inability of the S fibril- and MSA-derived strains to sequester α-syn into dense LB-like aggregates may also contribute to their faster propagation rates.

The biochemical and pathological properties of the S fibril-derived strain (i.e. comparatively short disease incubation periods, hind-limb paralysis phenotype, lack of hippocampal PSyn pathology, ring-like PSyn aggregates in neurons, and α-syn aggregates with low conformational stability) were similar, if not identical, to those of the MSA strain. Similarly, the properties of the NS fibril-derived strain (i.e. relatively longer disease incubation periods, hind-limb shaking phenotype, abundant hippocampal, cortical and olfactory bulb PSyn pathology, LB-like aggregates in neurons, and α-syn aggregates with intermediate conformational stability) were highly reminiscent of the $M83^{+/+}$ strain. At the current time, we cannot conclusively determine whether either of these pairs constitutes the same strain as opposed to unique strains with overlapping properties. It is possible that TgM83 mice are only able to replicate a small number of distinct α-syn strains[47], and that all strains will propagate as either an S fibril- or an NS fibril-like strain, depending on their conformational properties. Indeed, PMCA fibrils, which possess biochemical characteristics distinct from both S and NS fibrils, produced a disease phenotype indistinguishable from that of S fibrils upon propagation in TgM83 mice. Hence, α-syn strains may be composed of an ensemble or "cloud" of distinct conformational states, similar to what has been proposed for prion strains[48]. Propagation of recombinant α-syn strains in TgM83 mice may lead to selection of a minor component of the ensemble that is more compatible with the new host. This could also explain why α-syn aggregates in MSA patients are predominantly found within oligodendrocytes yet MSA-inoculated TgM83 mice exhibit only neuronal α-syn pathology[10, 11].

Two potential hypotheses have been put forward to explain the apparent spreading of α-syn aggregates within the brains of PD patients[49, 50]. The first, the selective neuronal vulnerability hypothesis, contends that α-syn aggregates appear first in cells that are most vulnerable to disease-associated toxicity and then appear later in less vulnerable cells once the disease has advanced. The second mechanism, the prion-like propagation theory, argues that α-syn aggregates directly transfer between neurons, acting as seeds for the generation of new aggregates in recipient cells. That the conformational and pathological properties of α-syn strains were faithfully maintained upon serial propagation argues that prion-like conformational templating, which requires physical contact between seed and substrate, occurred. However, the differential cellular tropism of α-syn strains argues that not all cells are equally susceptible to developing specific types of α-syn pathology. Thus, our results suggest that both prion-like spreading and selective vulnerability contribute to the temporal and spatial evolution of α-syn pathology within the brain.

Methods

For additional information, please see the online Life Sciences Reporting Summary

Expression and purification of recombinant α-syn

Untagged full-length human α-syn (residues 1-140), either wild-type or containing the A53T mutation, was inserted into the pET-28a vector (EMD Millipore) and then expressed and purified from *E. coli* strain BL21(DE3) using an established protocol[51]. Briefly, α-syn expression was induced for 2.5 h using isopropyl β-D-1-thiogalactopyranoside (IPTG) and then cell pellets were collected by centrifugation at 5,000x *g*. Pellets were washed in phosphate-buffered saline (PBS) and then spun down again at the same speed. Next, pellets were resuspended in PBS containing 1 mM phenylmethylsulfonyl fluoride (PMSF), lysed using a tip sonicator (18% amplitude, 6 pulses of 25 s with 2 min rest on ice in between), and then boiled for 15 min. Debris was pelleted by centrifugation at 10,000x *g* for 10 min, and then the supernatant was clarified by ultracentrifugation (150,000x *g* for 30 min) followed by dialysis against 50 mM Tris-HCl, pH 8.3. α-Syn was then purified by fast protein liquid chromatography using a Mono Q anion exchange column (GE Healthcare) and eluted using a linear gradient of 0 to 500 mM NaCl in 50 mM Tris-HCl, pH 8.3. The purity of eluted fractions was analyzed by sodium dodecyl sulfate polyacrylamide gel electrophoresis (SDS-PAGE) and Coomassie blue staining, and then fractions of sufficient purity were pooled and dialyzed against 20 mM Tris-HCl, pH 7.4. The concentration of purified α-syn was determined by measuring absorbance at 280 nm using a NanoDrop spectrophotometer (extinction coefficient = 5960), and then the purified protein was aliquoted, flash frozen, and stored at -80 °C.

Generation of α-syn fibrils

Our goal was to produce different preparations of recombinant α-syn fibrils that exhibited divergent conformational properties. To this end, we screened several different buffers and found that polymerization in the presence or absence of sodium chloride produced conformationally unique fibrils. Salt (S) and No Salt (NS) fibrils were generated by incubating recombinant α-syn at a concentration of 1 mg/mL (69 μM) at 37 °C with continuous shaking (600 rpm using an Eppendorf Thermomixer F1.5) for 7 days. S fibrils were prepared in a buffer containing 20 mM Tris-HCl, pH 7.4 and 100 mM NaCl whereas No Salt (NS) fibrils were prepared in a buffer containing 20 mM Tris-HCl, pH 7.4. Fibril formation was confirmed using a Thioflavin T (ThT) fluorescence assay. Briefly, fibrils were diluted into a buffer containing 10 μM ThT (SigmaAldrich #T3516) and then fluorescence was measured using excitation and emission wavelengths of 444 and 485 nm, respectively. To analyze the kinetics of fibril formation for S and NS fibrils, recombinant α-syn (1 mg/mL) was prepared in 20 mM Tris-HCl, pH 7.4 and 10 μM ThT with or without the addition of 100 mM NaCl. Protein was placed into the wells of a black 96-well clear-bottom microplate and then the plate was inserted into a BMG CLARIOstar microplate reader. Samples were incubated at 37 °C with continuous shaking (600 rpm; double orbital) for 12 days and ThT fluorescence (excitation: 444 ± 5 nm; emission: 485 ± 5 nm) was measured every 5 min. A gain setting of 1500 was used. Non-linear regression was used to fit the kinetic curves to a sigmoidal dose-response (variable slope) equation in GraphPad Prism, and then lag phases were calculated using the equation: $T_{50} - [1/(2*k)]$, where T_{50} is the time at which fluorescence is halfway between the baseline and plateau values, and k is the Hill slope. Lag phases were compared using a two-tailed, unpaired *t*-test. ThT fluorescence

values at different timepoints were compared by two-way analysis of variance (ANOVA) with Sidak's multiple comparisons test.

Protein misfolding cyclic amplification (PMCA) fibrils were generated by preparing recombinant α-syn at a concentration of 1 mg/mL in a buffer containing 20 mM Tris-HCl, pH 7.4 and 100 mM NaCl. Samples were placed in thin-walled polymerase chain reaction (PCR) microtubes and then positioned in a microtube holder (QSonica #444) suspended over a microplate horn sonicator (QSonica #431MPX). The bottoms of the tubes were submerged in water that was kept at 37 °C and was continually circulated for the duration of the experiment using a recirculating chiller (QSonica #4900-110). Samples were subjected to repeating cycles of 29 min 40 s of incubation and 20 s sonication (70% amplitude using a QSonica Q700 sonicator) over a period of two days.

Electron microscopy

Negative stain electron microscopy was used to examine the ultrastructural characteristics of S, NS, and PMCA fibrils. Aliquots (5 μL of 69 μM α-syn fibril preparations) containing recombinant α-syn fibrils were loaded on to freshly glow discharged 400 mesh carbon-coated copper grids (Electron Microscopy Sciences) and adsorbed for 1 minute. Grids were then washed with 50 μL each of 0.1 M and 0.01 M ammonium acetate and stained with 2x50 μL of freshly filtered 2% uranyl acetate. Once dry, grids were visualized with a Technai G20 transmission electron microscope (Thermo Fisher FEI) using an acceleration voltage of 200kV. Electron micrographs were recorded with an Eagle 4kx4k CCD camera (Thermo Fisher FEI). Fibril lengths were measured for a total of 62 S fibrils and 47 NS fibrils stemming from three independent fibril preparations. No overlapping or otherwise obscured fibrils were included in the length measurements. Measurements were determined in Adobe Photoshop software using the "Ruler" tool, which allows single pixel accuracy in the measurements with ~0.5 nm / pixel at the image magnification that was used. Mean fibril lengths in three independent preparations were compared using a two-tailed, unpaired *t*-test.

Proteinase K (PK) digestion of fibrils

Fibrils were diluted into 1X detergent buffer [0.5% (v/v) Nonidet P-40, 0.5% (w/v) sodium deoxycholate in PBS] containing PK (Thermo Scientific #EO0491) at a concentration of 50 μg/mL (PK:protein ratio of 1:1) and then incubated at 37 °C for 1 h with continuous shaking. Digestions were halted by adding PMSF to a final concentration of 4 mM and then samples were ultracentrifuged at 100,000x *g* for 1 h at 4 °C. The supernatant was discarded, and the pellets were resuspended by boiling in 1X Bolt lithium dodecyl sulfate (LDS) sample buffer (Thermo Scientific) containing 2.5% (v/v) β-mercaptoethanol ("loading buffer"). Samples were then analyzed by SDS-PAGE followed by silver staining.

SDS-PAGE and immunoblotting

Samples were prepared in loading buffer, boiled, and then run on either 4-12%, 10%, or 12% Bolt Bis-Tris Plus gels (Thermo Scientific) at 165 V for 35 min. The Thermo Scientific Pierce Silver Stain Kit and Bio-Safe Coomassie stain (Bio-Rad) were used for silver stains and Coomassie blue stains, respectively. For immunoblotting, proteins were transferred to 0.45 μm pore polyvinylidene fluoride (PVDF) membranes in transfer buffer [25 mM Tris pH

8.3, 0.192 M glycine, 20% (v/v) methanol] at 35 V for 1 h. The membranes were then incubated in 0.4% (v/v) paraformaldehyde in PBS for 30 min at room temperature to cross-link proteins to the membrane[52]. Membranes were blocked with blocking buffer [5% (w/v) skim milk in 1X TBS containing 0.05% (v/v) Tween-20 (TBST)] for 1 h at room temperature and then incubated overnight at 4 °C with primary antibody diluted in blocking buffer. The following primary antibodies were used: anti-Ser129-phosphorylated α-syn (PSyn) EP1536Y (Abcam #ab51253; 1:4,000 dilution), anti-α-syn Syn-1 (BD Biosciences #610786; 1:10,000 dilution), anti-human α-syn MJFR1 (Abcam #ab138501; 1:10,000 dilution), or anti-murine α-syn D37A6 (Cell Signaling Technology #4179; 1:10,000 dilution). Following 3 washes with TBST, the membranes were incubated with horseradish peroxidase-conjugated secondary antibodies (Bio-Rad #172-1019 or 172-1011) diluted 1:10,000 in blocking buffer for 1 h at room temperature. Following 3 washes with TBST, blots were developed using Western Lightning enhanced chemiluminescence (ECL) Pro (PerkinElmer) and either exposed to x-ray film or imaged using a LiCor Odyssey Fc system.

Curcumin dye-binding assay

Based on the recent demonstration that curcumin can be used as a conformation-sensitive probe for discriminating different types of Aβ fibrils[28], we developed a fluorescence spectral assay for α-syn fibrils using this dye. Reactions were prepared using 10 μM α-syn (either S fibrils, NS fibrils, or non-polymerized α-syn prepared in matching buffer) and curcumin (SigmaAldrich #C1386) at a final concentration of 5 μM in a total volume of 100 μL. Samples were then incubated at room temperature with shaking (850 rpm) for 15 min. Unbound dye was removed by dialyzing against dH_2O for ~50 min using Slide-A-Lyzer Mini dialysis tubes with a 10 kDa molecular weight cut-off (Thermo Scientific #69570). Samples were then placed into black 96-well clear-bottom half-area plates (Greiner), and fluorescent emission spectra (460 ± 5 to 625 ± 5 nm) following excitation at 432 ± 7.5 nm were recorded using a BMG CLARIOstar microplate reader with the gain set at 2000. Background fluorescence was subtracted using samples containing only curcumin that had been processed identically. For comparison of spectra, fluorescence values were normalized to the highest signal obtained within the spectrum (which was set at 1.0).

Cultured cell α-syn aggregation assay

A polyclonal HEK293 cell line stably expressing A53T-mutant human α-syn tagged at its C-terminus with yellow fluorescent protein (YFP)[29] was generously provided by Marc Diamond (UT Southwestern). These cells were cultured in growth medium [Dulbecco's Modified Eagle Medium (DMEM) containing 10% (v/v) fetal bovine serum, 1x GlutaMAX, and 0.2x penicillin/streptomycin] and maintained in a humidified 37 °C/5% CO_2 environment. For fibril transductions, equal volumes of Lipofectamine-2000 (Thermo Scientific) and α-syn fibril solutions, both diluted in Opti-MEM medium, were combined to give final concentrations of 2.8% (v/v) Lipofectamine-2000 and 1 μM total α-syn, and then incubated for 20 min to permit liposome formation. During this incubation, cells were trypsinized and then plated at a density of 20,000 cells/well in 24-well plates containing coverslips coated with poly-D-lysine. Transduction mixture (200 μL/well) was added and then the cells were incubated for 4 h. The transduction media was then removed and, without additional washes, replaced with growth medium and returned to the incubator for

an additional 20 h. Cells were fixed with methanol at -30 °C for 15 min, washed 3 times with PBS, and the coverslips were mounted on glass slides with ProLong Diamond Antifade Mountant containing 4',6-diamidino-2-phenylindole (DAPI; Thermo Scientific). Slides were allowed to dry overnight and then imaged used a Leica TCS SP8 confocal microscope. Images were processed using ImageJ and Adobe Photoshop.

For quantification of aggregate morphology, fibril-transduced cells were prepared as above with the exception that cells were fixed with 4% (w/v) paraformaldehyde for 15 min. Slides were viewed using a 40x objective on a Leica DM6000B microscope. For each replicate, four random fields were chosen and the number of aggregates exhibiting the "globular" or "thread-like" morphology were counted. These values were summed and converted to percentage of total aggregates. For both S- and NS-fibril treated cells, four independent replicates were analyzed. Aggregate morphologies were compared using a two-tailed *t*-test.

Fibril conformation stability assay (CSA)

Twenty microliters of 2X guanidine hydrochloride (GdnHCl) stocks were added to an equal volume of recombinant α-syn fibrils (5 μL of 1mg/mL fibrils plus 15 μL detergent buffer) to generate final GdnHCl concentrations of 1, 1.5, 2, 2.5, 3, 3.5, and 4 M. To generate the "0 M GdnHCl" sample, 20 μL of dH_20 was added. Samples were then incubated at room temperature for 2 h with continuous shaking (800 rpm). GdnHCl concentrations were then normalized to 0.4 M and the samples were ultracentrifuged at 100,000x *g* for 1 h at 4 °C using a TLA-55 rotor (Beckman). Supernatants were discarded and the pellets resuspended by boiling in loading buffer. Levels of residual α-syn were determined by SDS-PAGE followed by either immunoblotting or Coomassie blue staining. Densitometry was performed using ImageJ and values were normalized to the sample with the highest intensity, which was set at 100%. $GdnHCl_{50}$ values, the concentration of GdnHCl at which 50% of the aggregates are solubilized, were determined by non-linear regression using the sigmoidal dose-response (variable slope) equation in GraphPad Prism with the top and bottom values fixed at 100 and 0, respectively. $GdnHCl_{50}$ values were compared using a two-tailed, unpaired *t*-test. To generate denaturation curves, values for independent replicates were averaged and then normalized to the "0 M GdnHCl" value, which was set at 100%.

Single-molecule measurement of α-syn fibril doubling time

Fibril seeds were sonicated for 1 min at 60 W power and then added at a concentration of 0.35% (w/v) to a 300 μL solution of monomeric recombinant A53T-mutant α-syn (70 μM) prepared in PBS containing 0.01% (v/v) sodium azide. Seeding reactions were carried out at 37 °C with continuous shaking (200 rpm), and aliquots were withdrawn at defined timepoints for analysis by total internal reflection fluorescence (TIRF) microscopy. Protein aliquots were diluted to a final concentration of 100 nM in PBS containing 25 μM ThT and then loaded onto a slide. Borosilicate glass coverslips were cleaned by argon plasma for 1 h and then attached to Frame-Seal slide chambers (9 x 9 mm), with the surface coated with poly-L-lysine (MW = 150,000 - 300,000, 0.01% (v/v)). Imaging was performed using a home-built TIRF microscopy setup. A 35 mW diode laser with a wavelength of 405 nm was passed through a single-band bandpass filter then directed into a 60x magnification oil-

immersion TIRF objective (NA = 1.49) mounted on an inverted microscope. The TIRF mode was achieved by adjusting the position of the aligned laser beam before it entered the objective, illuminating samples mixed with ThT molecules. The emitted fluorescence was collected by the same objective, separated by a dichroic mirror from the returning TIR beam, and then passed through an emission filter. The fluorescence signal was recorded by an EMCCD camera. Each recorded area contained a 3 x 3 grid (i.e. 9 images were recorded sequentially at adjacent positions), in which the dimensions of a single image were 512 x 512 pixels (i.e. 110 x 110 μm^2), with a gap distance of 150 μm. For each time point in the kinetic measurements, three random areas (i.e. 27 images) were recorded. Each image sequence was acquired as a 100-framed stack at 30 frames per second. Individual image data were averaged over all the frames by ImageJ (http://imagej.nih.gov/ij/) and the images were then analyzed with a custom-written MATLAB script, which has been uploaded to Github (https://github.com/jason82133/Particle-measurement.git). For particle identification, background was removed by applying 2D Gaussian blur and bandpass filters. Boundaries for individual particles were identified by applying a black/white filter (i.e. an intensity threshold), while their positions were located by calculating centroid positions. Particle length was measured, using built-in algorithms by thinning individual boundaries of particles, and then calculated with the image pixel size of 235 nm.

To extract multiplication rates from the *in vitro* data of average length as a function of time, the system was modelled by the differential equations describing linear polymerisation with monomer concentration-independent multiplication[53]:

$$\frac{dM}{dt} = 2(k_e m(t) - k_{off})P(t)$$

$$\frac{dP}{dt} = k_f M(t)$$

where M(t) is the mass concentration of aggregates and P(t) is the number concentration of aggregates. Thus, the average number of monomers per aggregate is given by M(t)/P(t). k_e, k_{off} and k_f are the rate constants of elongation, depolymerization, and fragmentation respectively. From these constants, the doubling time (t_2), i.e. the time taken to double the number of aggregates at a given monomer concentration m, is given by

$$t_2 = \frac{\ln(2)}{\sqrt{2 k_e m k_f}}$$

To convert the measured length (in nm) to the number of monomers per aggregate an additional parameter, the number of monomers per unit length of fibril, is needed (relative differences between the multiplication rate are insensitive to the precise value of this parameter as long as it is the same for the systems being compared). The data were fit by numerical integration of the above differential equations, with 3 free fitting parameters (k_e, k_f and the number of monomers per unit length of the fibril). The depolymerization rate was expressed in terms of the monomer concentration at equilibrium, and the elongation rate k_{off}

= m_{equ}*k_e., thus reducing the number of fitting parameters to 3 overall. The initial concentration of fibrils, M(t=0), was 0.245 μM and the initial fibril length was determined from the average length at time 0.

Mice

Homozygous M83 transgenic mice (M83$^{+/+}$), which express A53T-mutant human α-syn under the control of the mouse prion protein promoter[26] on a mixed C57BL6/C3H background, and B6C3F1 non-transgenic mice were purchased from Jackson Lab (stock numbers 004479 and 100010, respectively). These two lines were intercrossed to generate hemizygous TgM83 mice, which were housed at 4-5 animals per cage. Mice were maintained on a 12 h light/12 h dark cycle and were given unlimited access to food and water. All mouse experiments were performed in accordance with guidelines set by the Canadian Council on Animal Care under a protocol (AUP #4263.6) approved by the University Health Network Animal Care Committee.

Tissue samples

Human synucleinopathy samples were provided by the Massachusetts Alzheimer's Disease Research Center and Alzheimer's disease samples were obtained from the Canadian Brain Tissue Bank (CBTB). Informed consent was obtained at the point of tissue collection. A list of brain tissues used is given in Supplementary Table 2. The use of human tissue was in accordance with guidelines provided by the University of Toronto, and all relevant ethical regulations were followed. Spontaneously ill M83$^{+/+}$ mice were euthanized once prominent hind-limb paralysis and bradykinesia as well as concomitant weight loss were observed. Mice were perfused with saline, and then the brain was removed and bisected parasagittally. The right half of the brain was fixed in 10% neutral buffered formalin and the left half was frozen and stored at -80 °C. The M83$^{+/+}$ sample used for inoculation studies was from a male mouse that was euthanized at 371 days of age. Brain homogenates from frozen MSA, DLB, AD, or M83$^{+/+}$ tissue [10% (w/v) prepared in calcium- and magnesium-free PBS] were generated using a Minilys homogenizer and CK14 soft tissue homogenizing tubes (Bertin Corp.). Homogenates were aliquoted and then stored at -80 °C.

Intracerebral inoculations

Inoculations were performed as follows: ~5-week-old hemizygous M83 mice were anaesthetized and then inoculated non-stereotactically, using a tuberculin syringe with an attached 27 gauge, 0.5 in needle (BD Biosciences #305945), with 30 μL of sample at a depth of ~3 mm into the right cerebral hemisphere of the brain. This region corresponds to the hippocampus/thalamus. For inoculations with recombinant α-syn preparations (either S fibrils, NS fibrils, or monomeric α-syn), each mouse received 1 μg of total α-syn diluted in inoculum diluent buffer [5% (w/v) BSA prepared in sterile PBS]. For PBS inoculations, sterile PBS was diluted 1:10 in inoculum diluent buffer prior to inoculation. For inoculations with brain-derived samples, homogenates were diluted to 1% (w/v) in inoculum diluent buffer prior to injection. For serial passaging experiments, brain homogenates from previously inoculated hemizygous TgM83 mice were used. We estimate that for the serial transmission experiments, mice received ~10-fold less α-syn aggregates than for the original fibril inoculations. Both male and female mice were used for inoculation studies. The sex

distribution for individual experiments is shown in Supplementary Table 3. Mice were randomly assigned to the experimental groups. No statistical methods were used to pre-determine mouse numbers for inoculation experiments, but our sample sizes are similar to those reported in previous publications[10, 11]. Inoculated mice were monitored daily for routine health and assessed 2-3 times per week for signs of neurological illness. Mice were euthanized after progressing to end-stage disease, which was defined as either prominent hind-limb paralysis with reduced ambulation, or hind-limb shaking accompanied by obvious weight loss and kyphosis. Disease incubation periods were compared by one-way ANOVA with Tukey's multiple comparisons test. Following transcardiac perfusion with saline solution, brains were divided parasagittally. The left half of the brain was frozen and stored at -80 °C for biochemical experiments, and the right half was fixed in 10% neutral buffered formalin for neuropathology. Some inoculated mice were found dead in the absence of neurological signs or were euthanized due to intercurrent illness (Supplementary Table 4). These mice were omitted from the study.

Protease digestion assays

Brain homogenates [10% (w/v)] were prepared in PBS using a Minilys homogenizer and CK14 homogenizing tubes. Nine volumes of brain homogenate were then mixed with one volume of 10X detergent buffer [5% (v/v) Nonidet P-40, 5% (w/v) sodium deoxycholate in PBS] containing Pierce Universal Nuclease (ThermoFisher #88701) and Halt Phosphatase Inhibitor (ThermoFisher #78420), and then incubated on ice for 20 min. Samples were clarified by centrifugation at 1000x *g* for 5 min at 4 °C to generate detergent-extracted brain homogenate. For thermolysin (SigmaAldrich #T7902) digestions, extracts were treated with 50 μg/mL protease (TL:protein ratio of 1:100) at 37 °C for 1 h with constant agitation (600 rpm). Digestions were terminated by the addition of ethylenediaminetetraacetic acid (EDTA) to a final concentration of 5 mM. For PK digestions, detergent-extracted brain homogenates were treated with 100 μg/mL PK (PK:protein ratio of 1:50) at 37 °C for 1 h with constant agitation (600 rpm). Digestions were terminated by the addition of PMSF to a final concentration of 4 mM. Following digestion, samples were ultracentrifuged at 100,000x *g* for 1 h at 4 °C. The supernatant was discarded, and the pellets were resuspended by boiling in loading buffer. Samples were then analyzed by SDS-PAGE followed by immunoblotting.

CSA for α-syn aggregates in brain extracts

Detergent-extracted brain homogenates were generated as described above. Twenty microliters of 2X guanidine hydrochloride (GdnHCl) stocks were added to an equal volume of brain extract to generate final GdnHCl concentrations of 1, 1.5, 2, 2.5, 3, 3.5, and 4 M. To generate the "0 M GdnHCl" sample, 20 μL of dH_20 was added. For some CSAs on brain extract from DLB and AD patients, an extended range CSA was performed with final GdnHCl concentrations of 1, 2, 2.5, 3, 3.5, 4, 4.5, 5, 5.5, and 6 M. Samples were then incubated at room temperature for 2 h with continuous shaking (800 rpm). GdnHCl concentrations were then normalized to 0.4 M and the samples were ultracentrifuged at 100,000x *g* for 1 h at 4 °C using a TLA-55 rotor (Beckman). Supernatants were discarded and the pellets resuspended by boiling in loading buffer. Levels of residual α-syn were determined by SDS-PAGE followed by immunoblotting. Densitometry was performed using ImageJ and values were normalized to the sample with the highest intensity, which was set

at 100%. $GdnHCl_{50}$ values were determined by non-linear regression using the sigmoidal dose-response (variable slope) equation in GraphPad Prism with the top and bottom values fixed at 100 and 0, respectively. $GdnHCl_{50}$ values were compared using two-tailed, unpaired *t*-tests or by one-way ANOVA with Tukey's multiple comparisons test. To generate denaturation curves, values for independent replicates were averaged and then normalized to the "0 M GdnHCl" value (or the "1M GdnHCl" value for the extended range CSA), which was set at 100%.

Immunohistochemistry

Formalin-fixed perfused mouse hemibrains were dehydrated through a graded series of ethanol using an automated tissue processor and then embedded in paraffin wax. Sagittal sections of 5 μm thickness at the midline of the brain (~0.5-1 mm lateral) were mounted on glass slides, deparaffinized, and then rehydrated using a graded series of ethanol for immunohistochemistry. Endogenous peroxidase activity was quenched by incubating the slides in 3% (v/v) H_2O_2 prepared in methanol for 25 min, and then slides were rinsed three times (5 min each) with dH_2O and once with PBS containing 0.05% (v/v) Tween-20 (PBS-T). Sections were blocked by incubation in 2.5% (v/v) normal horse serum for 60 min at room temperature. Immunohistochemistry was performed using the following antibodies: rabbit monoclonal anti-PSyn EP1536Y (Abcam #ab51253; 1:320,000 dilution) or mouse monoclonal anti-p62/SQSTM1 (Abcam #ab56416; 1:10,000 dilution). The EP1536Y antibody does not cross-react with phosphorylated neurofilaments[54]. Sections to be stained with the p62/SQSTM1 antibody were first subjected to heat-mediated antigen retrieval in 0.1 M citrate buffer (pH 6.0). All primary antibodies were diluted in antibody diluent (Dako #S080983-2), and stainings were performed overnight at 4 °C. Following three washes with PBS-T (5 min each), slides were processed using the ImmPress horseradish peroxidase-labeled horse anti-rabbit or anti-mouse detection kits (Vector Laboratories #MP-7401 or MP-7402), and then washed three times (5 min each) with PBS-T. Slides were developed using ImmPACT 3,3'-diaminobenzidine (DAB) peroxidase substrate (Vector Laboratories #SK-4105) for 1 min, washed with tap water for 10 min, counterstained with haematoxylin, and then mounted. Detection of PK-resistant α-syn species using the antibody LB509 (Thermo Scientific #180215; 1:500 dilution) was performed as previously described[55]. Brain sections were imaged using a Leica DM6000B microscope with either 20x, 40x, or 63x objectives in conjunction with Volocity software (version 6.3).

For semi-quantitative scoring of PSyn deposition in the brains of inoculated TgM83 mice, the following scoring system was utilized: 0, no PSyn deposition; 1, mild PSyn deposition; 2, moderate PSyn deposition; 3, intense PSyn deposition. PSyn deposition was scored in 9 different brain regions: olfactory bulb, frontal association cortex, parietal cortex, hippocampus, thalamus, hypothalamus, midbrain, cerebellar white matter, and brainstem. Patterns of PSyn deposition were compared by two-way ANOVA with Sidak's multiple comparisons test. For experiments in which the olfactory bulb was missing from a few mice, a mixed-effects model with Sidak's multiple comparisons test was used. PSyn-positive astrocyte counts were conducted in the thalamus and were compared by one-way ANOVA with Tukey's multiple comparisons test. For quantification of ring-like vs. LB-like PSyn deposits, counts were performed in the midbrain and the converted into percentage of total

aggregates (ring-like plus LB-like). Data were compared by one-way ANOVA followed by Tukey's multiple comparisons test.

For double-labeling of PSyn and glial fibrillary acidic protein (GFAP), sections were deparaffinized in xylene and rehydrated in decreasing concentrations of ethanol, followed by two washes with PBS. Epitope retrieval was performed by incubating the sections for 15 minutes in 0.1 M sodium citrate buffer (pH 6.0) in a steam sterilizer, followed by incubation in a blocking solution of 5% (v/v) donkey serum and 0.25% (v/v) Triton X-100 in PBS for 1 h at room temperature. The sections were then incubated with rabbit anti-PSyn EP1536Y (1:1,000 dilution) and goat anti-GFAP (Novus Biologicals #NB100-53809, 1:300 dilution) for 24 h at 4 °C. Following three washes with PBS, sections were incubated with Alexa Fluor 594-labeled donkey anti-rabbit IgG (Abcam #ab150076, 1:750 dilution) and Alexa Fluor 488-labeled donkey anti-goat IgG (Jackson ImmunoResearch Laboratories #705-545-003, 1:1,000 dilution) for 2 h at room temperature. Nuclei were counterstained with DAPI (Sigma-Aldrich #D9542, 1:10 000 dilution). Following three washes with PBS and then 0.1 M sodium phosphate, the sections were mounted using Prolong Diamond antifade mountant (Thermo Scientific #P36961). Images were acquired using a Zeiss LSM880 scanning confocal microscope couple to a CCD camera (Zeiss Axio Observer Z1) in conjunction with Zen software (Carl Zeiss). Images were processed using ImageJ and Adobe Photoshop.

Statistics and Reproducibility

All statistical analyses were performed using GraphPad Prism (v. 8.2) with a significance threshold of $P = 0.05$. Data were compared using unpaired two-tailed *t*-tests, one-way ANOVA with Tukey's multiple comparisons test, or two-way ANOVA with Sidak's multiple comparisons test, as described above. Data distribution was assumed to be normal, but this was not formally tested. Data collection and analysis were not performed blind to the conditions of the experiments. All experiments on recombinant α-syn fibrils were performed using a minimum of 3 independent fibril preparations per strain. For neuropathological analysis, the brains from all inoculated mice were analyzed with the exception of the PMCA fibril second passage experiment, where 5 of 9 brains were examined. One brain from the third passage of the NS fibril-derived strain was unable to be collected for analysis. For the conformational stability assays, a minimum of 3 brains were analyzed per experimental condition. For non-quantitative experiments (thermolysin and proteinase K digestion assays), a minimum of 2 brains were analyzed from each experimental condition, and similar results were obtained for every sample within a group.

Extended Data

Europe PMC Funders Author Manuscripts

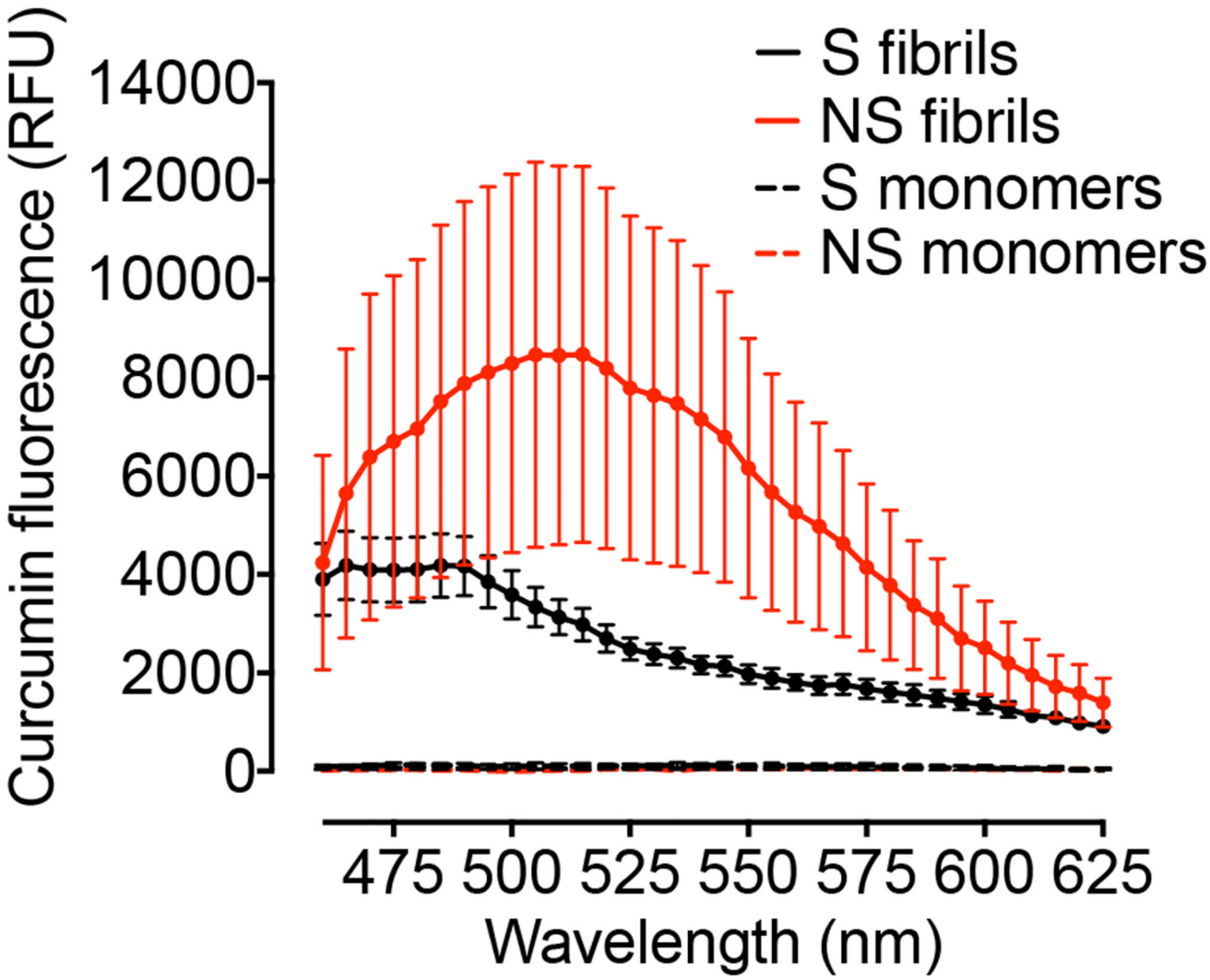

Extended Data Fig. 1. Non-normalized data for curcumin fluorescence spectral assay

S fibrils, NS fibrils, or non-polymerized (monomeric) forms of recombinant α-syn(A53T) were subjected to the curcumin dye-binding assay. Spectra were background-corrected but were not normalized. Only the fibrillar forms of α-syn gave appreciable signal, indicating that the assay is specific for aggregates. Each data point represents the mean relative fluorescence obtained from 3 biologically independent fibril preparations ± s.e.m.

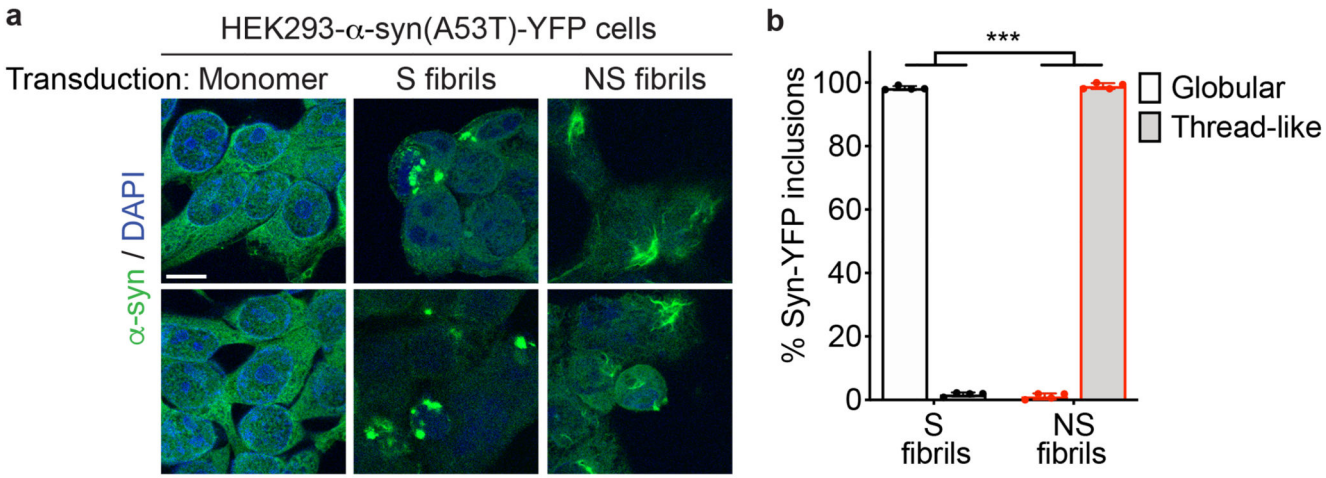

Extended Data Fig. 2. α-Syn fibril strains produce distinct inclusions in a cultured cell bioassay

a) HEK293 cells expressing YFP-tagged α-syn(A53T) were transduced with monomeric α-syn(A53T), S fibrils, or NS fibrils. Each image depicts representative cells following transduction with independent fibril preparations. Scale bar = 10 μm (applies to all images). **b**) Cells transduced with S fibrils predominantly develop "globular" inclusions whereas cells transduced with NS fibrils predominantly develop "thread-like" inclusions ($P = 2.8 \times 10^{-12}$, as determined by a two-tailed *t*-test). Data is mean ± s.e.m. from 4 biologically independent transductions.

Europe PMC Funders Author Manuscripts

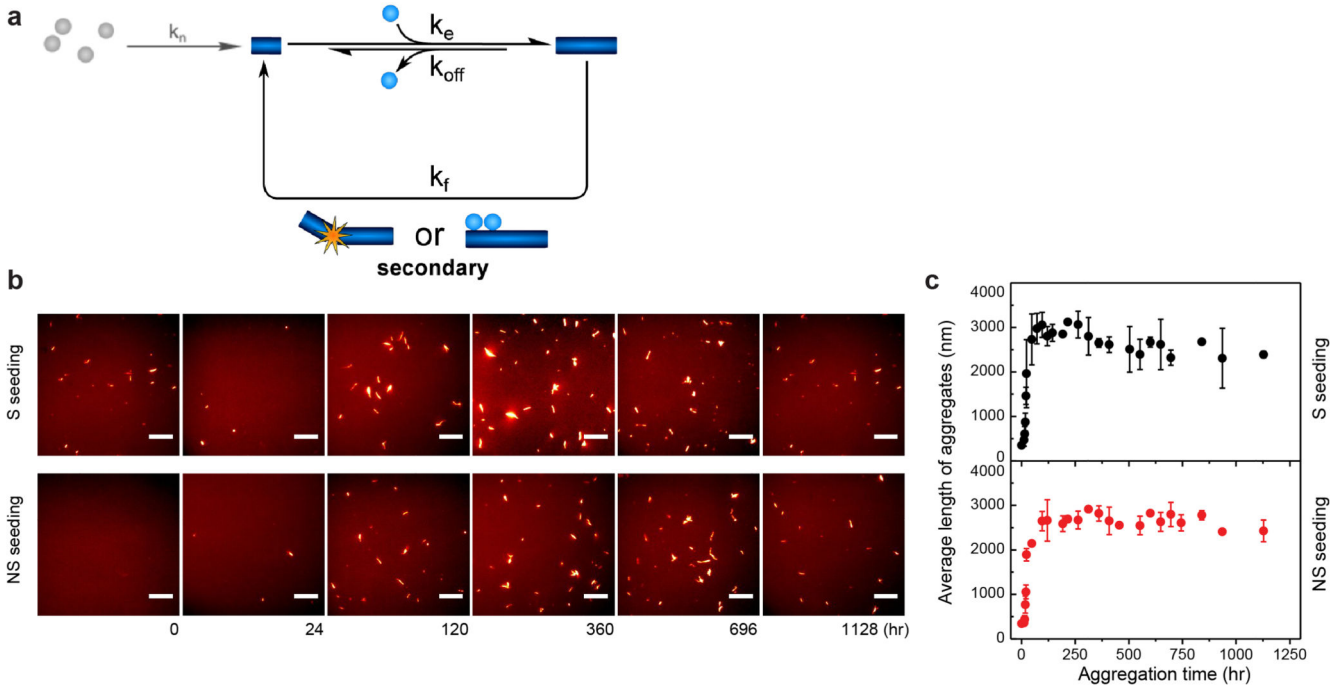

Extended Data Fig. 3. Single-molecule fibril seeding assay for measuring the doubling time of α-syn fibril strains

a) Schematic of fibril assembly and fragmentation model used to determine the doubling time for α-syn fibril strains. For a given concentration of monomeric α-syn(A53T), the doubling time (t_2) is determined by the rate constants for fibril elongation (k_e) and fragmentation (k_f). **b**) Representative ThT-stained total internal reflection fluorescence microscopy images at the indicated timepoints following seeding of monomeric α-syn(A53T) with S or NS fibrils. Scale bars = 10 μm. **c**) Single-molecule quantification of aggregate length as a function of time following seeding with S or NS fibrils. Each data point represents the mean ± s.e.m. from 3 independent seeding reactions.

Europe PMC Funders Author Manuscripts

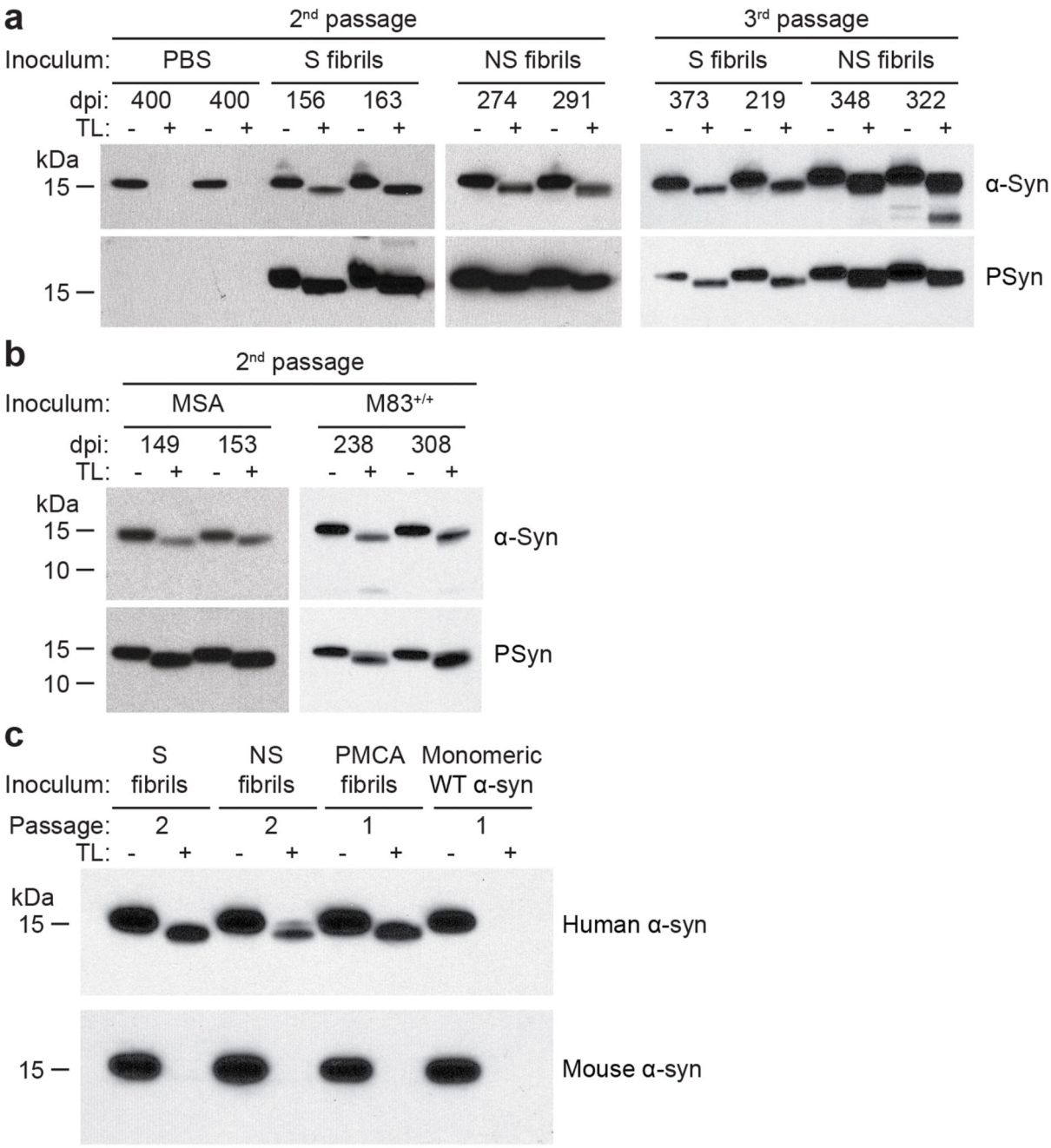

Extended Data Fig. 4. Additional thermolysin digestions of brain homogenates from inoculated TgM83 mice

a) Immunoblots of detergent-insoluble α-syn species in brain homogenates from the second or third passage of the S or NS fibril-derived strains in TgM83 mice, with or without digestion with thermolysin (TL). Brain homogenates from asymptomatic TgM83 mice from the second passage of PBS were used as a negative control. **b**) Immunoblots of detergent-insoluble α-syn species in brain homogenates from the second passage of the MSA- or $M83^{+/+}$-derived strains in TgM83 mice, with or without digestion with TL. In b and c, blots

Europe PMC Funders Author Manuscripts

were probed with antibodies to either total α-syn or PSyn. For each inoculum, results from two distinct mice are shown. dpi, days post-inoculation. **c**) Immunoblots of detergent-insoluble α-syn species in brain homogenates from TgM83 mice inoculated with the indicated α-syn preparations, with or without digestion with TL. Human α-syn was detected with the antibody MJFR1 and mouse α-syn was detected with the antibody D37A6. TL-resistant α-syn species were only present in the animals injected with α-syn aggregates and were only detectable with the antibody specific for human α-syn.

Europe PMC Funders Author Manuscripts

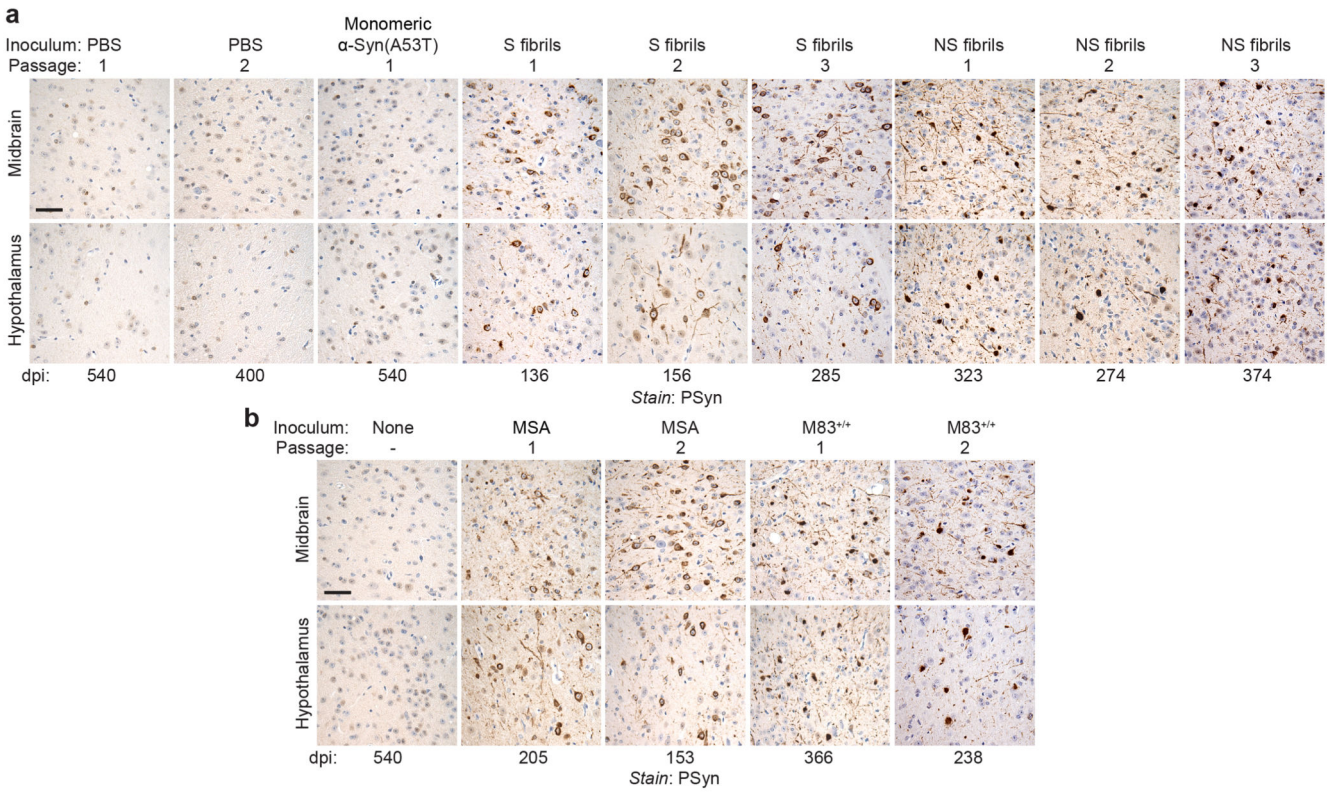

Extended Data Fig. 5. Phosphorylated α-syn (PSyn) deposition in the midbrain and hypothalamus of TgM83 mice injected with various α-syn strains.

a) Representative immunohistochemistry images for PSyn in midbrain and hypothalamus sections from asymptomatic TgM83 mice following inoculation with either PBS or monomeric α-syn, or from clinically ill mice inoculated with either the S fibril- or NS fibril-derived strains (first, second, or third passage). Scale bar = 50 μm (applies to all images). dpi, days post-inoculation. **b**) Representative immunohistochemistry images for PSyn in midbrain and hypothalamus sections from asymptomatic uninoculated TgM83 mice, or from clinically ill mice inoculated with either the MSA- or $M83^{+/+}$-derived strains (first or second passage). Scale bar = 50 μm (applies to all images).

Europe PMC Funders Author Manuscripts

Europe PMC Funders Author Manuscripts

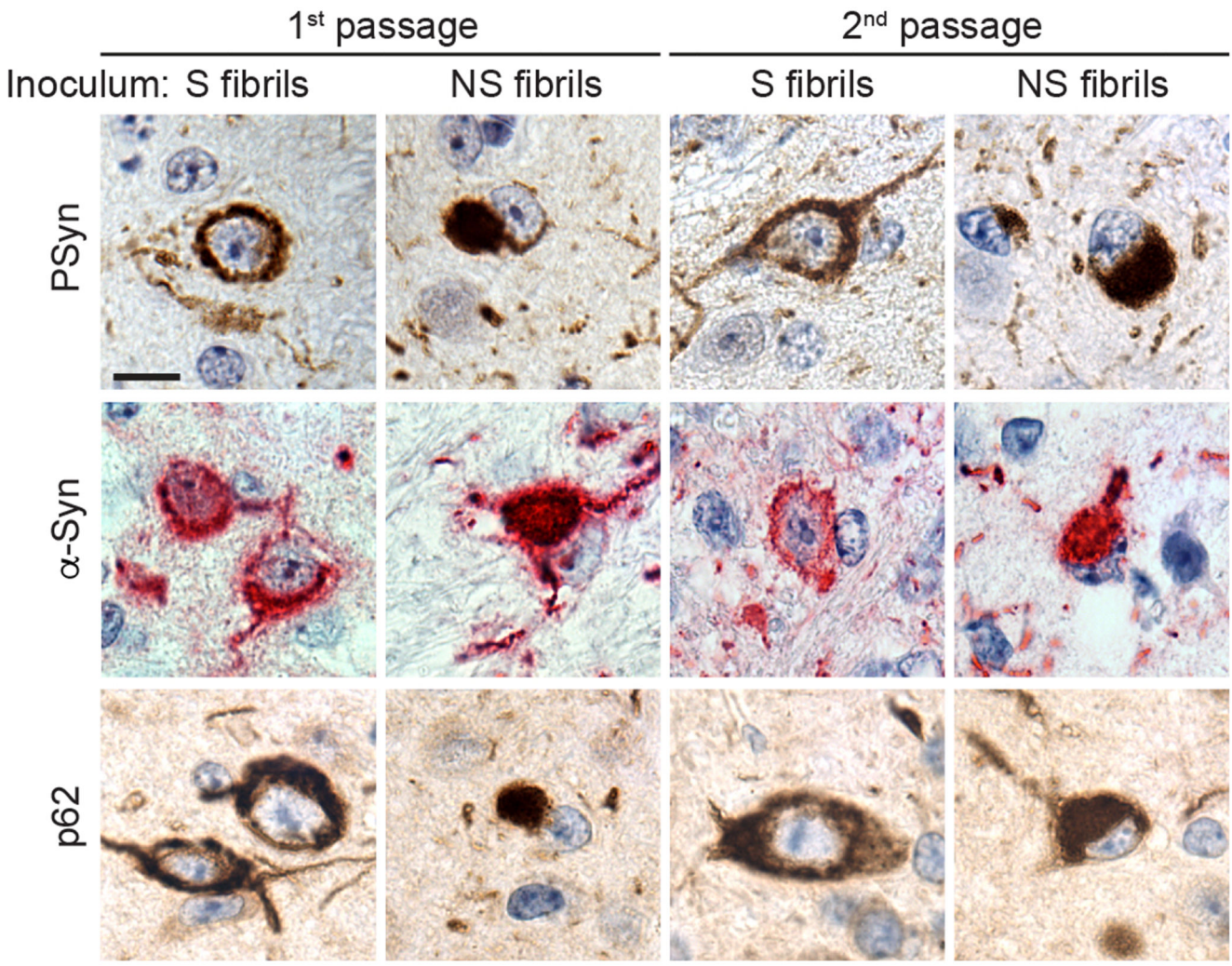

Extended Data Fig. 6. Additional immunohistochemical characterization of α-syn inclusions in TgM83 mice inoculated with the S or NS fibril-derived strains

Representative immunohistochemistry images for either PSyn (midbrain), PK-resistant total α-syn (hypothalamus), or p62 (midbrain) in brain sections from clinically ill TgM83 mice inoculated with either the S fibril- or NS fibril-derived strains (first or second passage). Scale bar = 10 μm (applies to all images). For each experimental group, stainings were performed on a minimum of two mice with similar results.

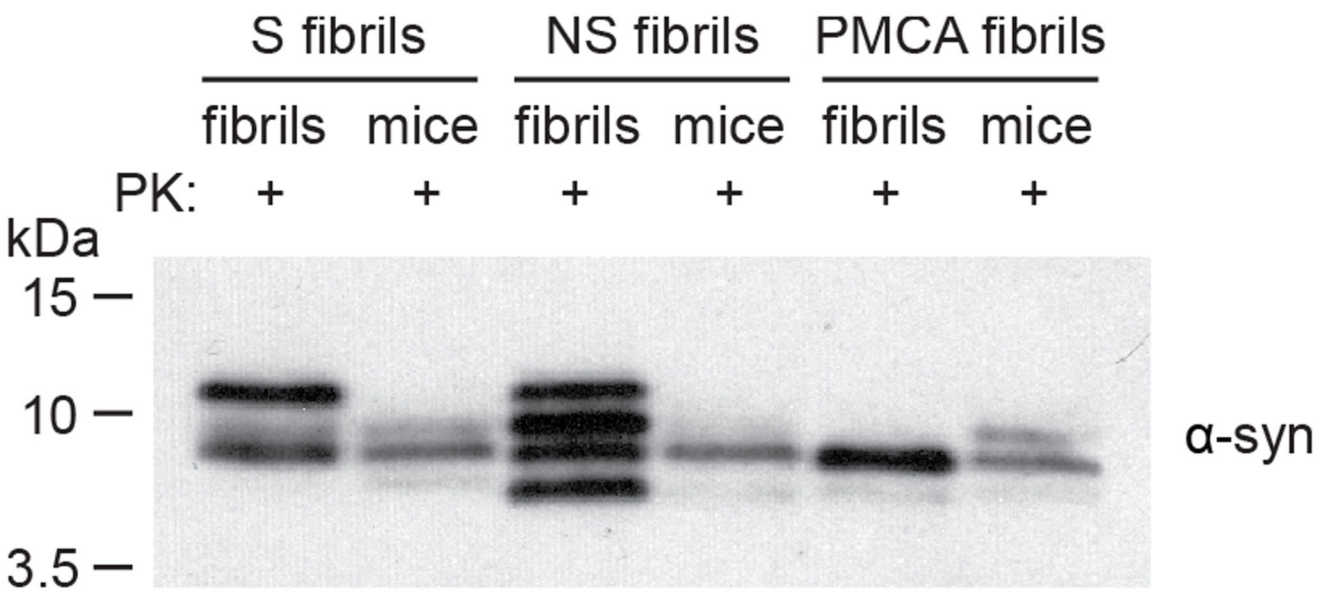

Extended Data Fig. 7. Comparison of PK-resistant α-syn species generated from recombinant α-syn fibril strains with α-syn species in brain homogenates from fibril-inoculated TgM83 mice

Immunoblot of detergent-insoluble α-syn species following digestion of recombinant fibrils or brain homogenates from fibril-inoculated TgM83 mice (first passage) with PK. PK-resistant α-syn was detected using the antibody Syn-1.

Europe PMC Funders Author Manuscripts

Europe PMC Funders Author Manuscripts

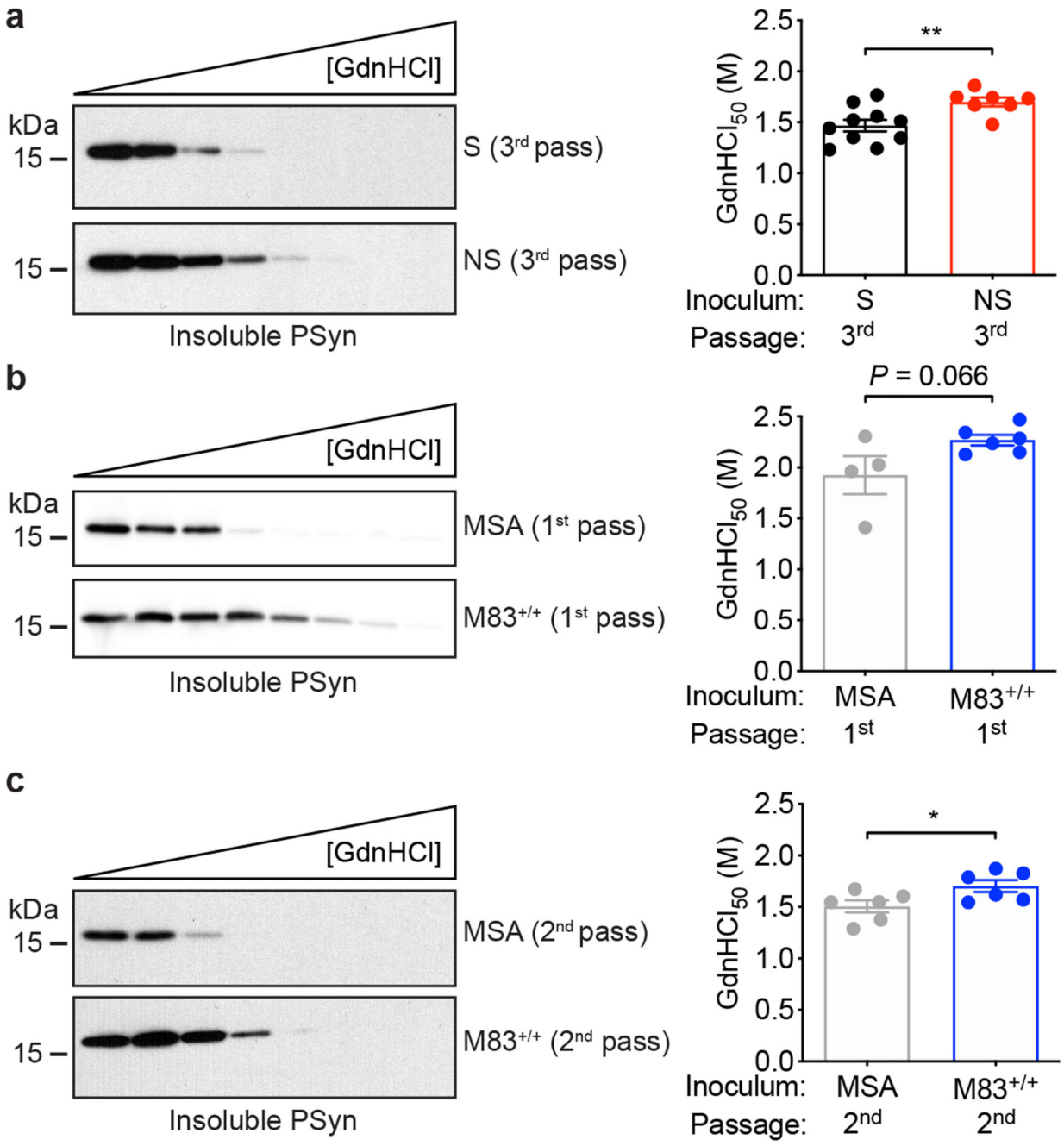

Extended Data Fig. 8. Additional conformational stability assay (CSA) data for α-syn species in brain homogenates from inoculated TgM83 mice

a) CSA for PSyn aggregates in clinically ill TgM83 mice inoculated with either the S or NS fibril-derived strains (third passage). Representative PSyn immunoblots and the resultant $GdnHCl_{50}$ values are shown. The PSyn aggregates in mice inoculated with the NS fibril-derived strain are significantly more stable ($P = 0.0091$). Data is mean ± s.e.m (n = 10 mice for the S strain and n = 7 mice for the NS strain). **b**) CSA for PSyn aggregates in clinically ill TgM83 mice inoculated with either MSA- or $M83^{+/+}$ brain extract (first passage).

Europe PMC Funders Author Manuscripts

Representative PSyn immunoblots and the resultant GdnHCl50 values are shown. Data is mean ± s.e.m (n = 4 for MSA-inoculated mice, n = 6 for $M83^{+/+}$-inoculated mice). **c**) CSA for PSyn aggregates in clinically ill TgM83 mice inoculated with either the MSA- or $M83^{+/+}$-derived strains (second passage). Representative PSyn immunoblots and the resultant $GdnHCl_{50}$ values are shown. The PSyn aggregates in mice inoculated with the $M83^{+/+}$-derived strain are significantly more stable ($P = 0.038$). Data is mean ± s.e.m (n = 6 for both groups of inoculated mice). All P values were obtained using a two-tailed t-test.

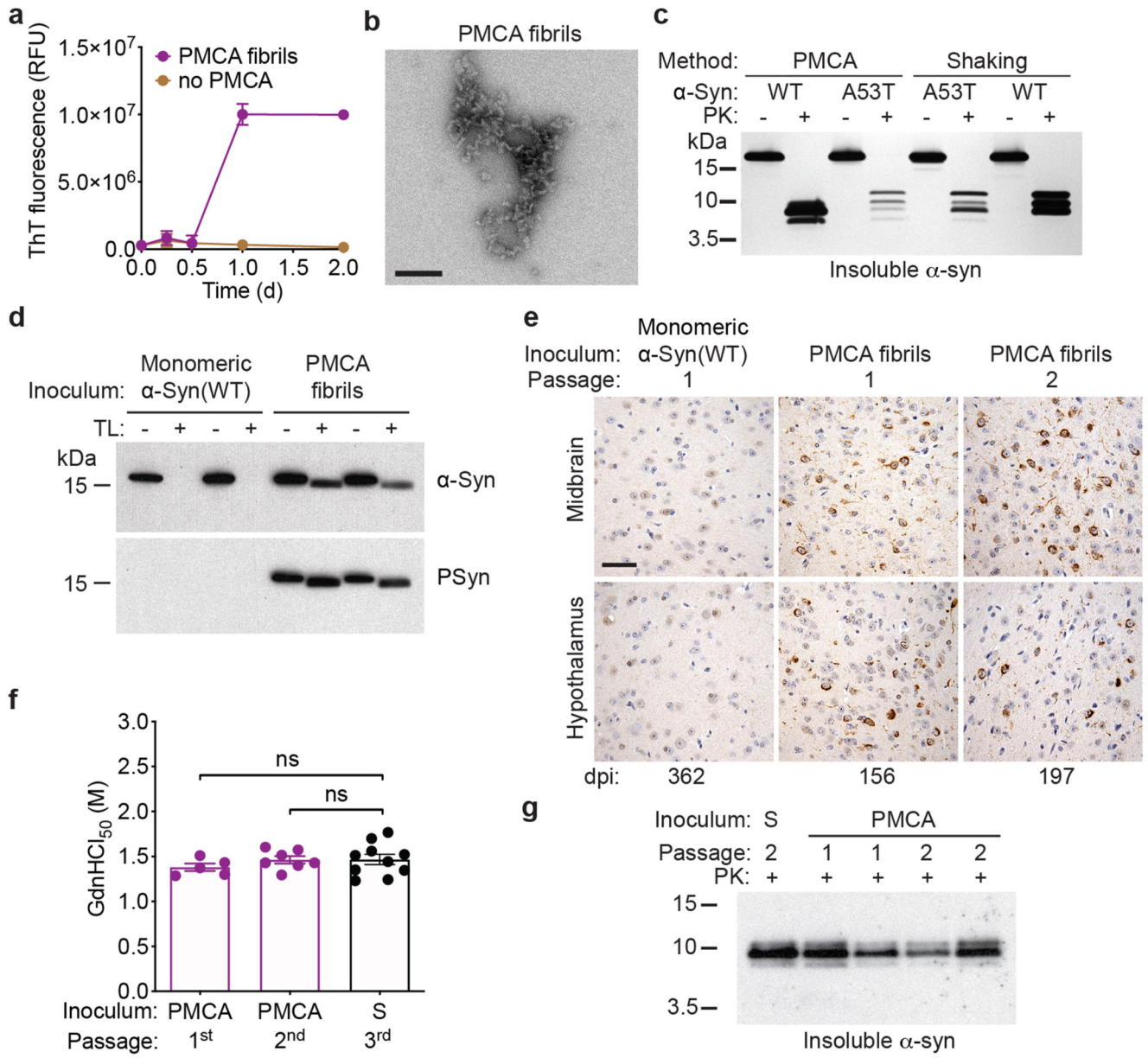

Extended Data Fig. 9. Additional characterization of PMCA-generated α-syn fibrils and PMCA fibril-inoculated TgM83 mice

a) Kinetics of fibril formation for PMCA fibrils in a ThT fluorescence assay. Reactions incubated at 37 ºC in the absence of shaking or sonication ("no PMCA") were used as a negative control. Each data point represents the mean ± s.e.m of 4 biologically independent replicates. **b**) Negative stain electron micrograph of PMCA fibrils. The PMCA procedure generated fibrils that were much shorter than either the S or NS fibrils (determined using 3 biologically independent fibril preparations). Scale bar = 200 nm. **c**) SDS-PAGE followed by silver staining of PK-digested α-syn fibril preparations. PMCA fibrils composed of wild-type (WT) α-syn exhibit a different banding pattern of insoluble PK-resistant α-syn species compared to S fibrils, NS fibrils, and PMCA fibrils composed of A53T-mutant α-syn. **d**)

Europe PMC Funders Author Manuscripts

Europe PMC Funders Author Manuscripts

Immunoblots of detergent-insoluble total α-syn and PSyn species in brain homogenates from two distinct asymptomatic monomer-inoculated mice or clinically ill PMCA fibril-inoculated mice (first passage), with or without digestion with TL. **e**) Representative immunohistochemistry images for PSyn in midbrain and hypothalamus sections from asymptomatic TgM83 mice following inoculation with monomeric α-syn, or from clinically ill mice inoculated with the PMCA fibril-derived strain (first or second passage). Scale bar = 50 μm (applies to all images). **f**) $GdnHCl_{50}$ values for PSyn aggregates in TgM83 mice inoculated with the PMCA fibril-derived strain (first or second passage) are not significantly (ns) different ($P = 0.52$ for first passage; $P = 0.99$ for second passage by one-way ANOVA with Tukey's multiple comparisons test) than for mice inoculated with the S fibril-derived strain (third passage). Data is mean ± s.e.m (n = 5 for first passage PMCA, n = 7 for second passage PMCA, and n = 10 for third passage S strain). **g**) Immunoblot of PK-digested and detergent-insoluble α-syn species in brain homogenates from clinically ill TgM83 mice inoculated with either the PMCA fibril-derived strain (first or second passage) or the S fibril-derived strain (second passage). Blot was probed with the Syn-1 antibody.

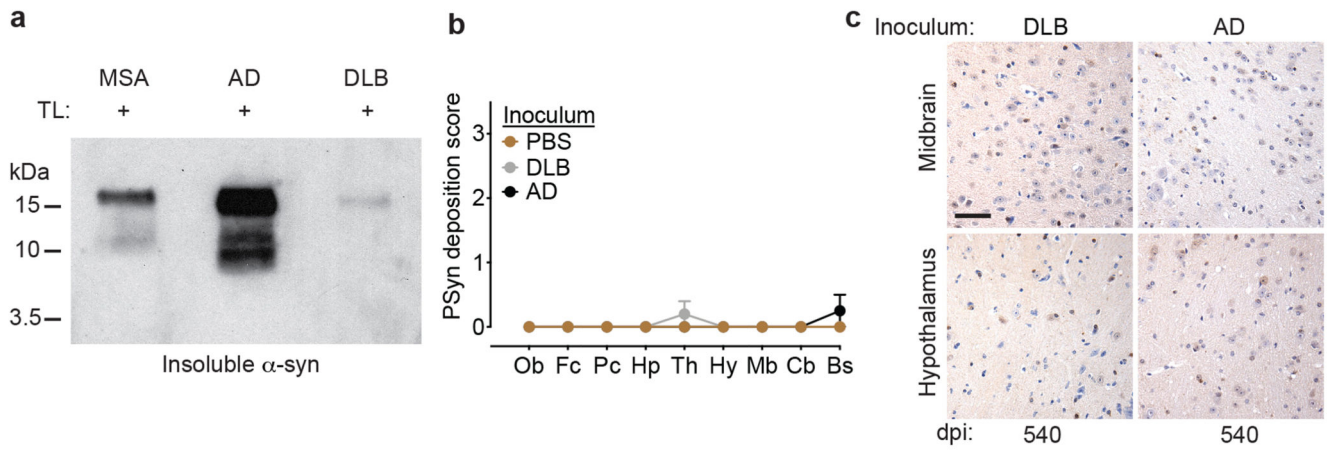

Extended Data Fig. 10. Absence of PSyn pathology in TgM83 mice inoculated with brain extract from a DLB patient or an AD patient with concomitant α-syn deposition

a) Thermolysin digestion of brain extracts from the three human synucleinopathy samples inoculated into TgM83 mice. α-Syn was detected using the antibody Syn-1. **b**) Semiquantitative PSyn deposition scoring (data are mean ± s.e.m.) within the indicated brain regions from asymptomatic TgM83 mice at 540 days following inoculation with PBS (first passage, n = 7), DLB brain extract (n = 5), or AD brain extract (n = 4). **c**) Representative immunohistochemistry images for PSyn in midbrain and hypothalamus sections from asymptomatic TgM83 mice following inoculation with DLB or AD brain extract. Scale bar = 50 μm (applies to all images).

Supplementary Material

Refer to Web version on PubMed Central for supplementary material.

Acknowledgments

The authors thank M. Diamond (UT Southwestern) for providing the HEK293 cells expressing YFP-tagged α-syn(A53T) as well as C. Sato and P. St. George-Hyslop for providing tissue from the Canadian Brain Tissue Bank. This work was supported by a new investigator award from Parkinson Canada/Pedalling for Parkinson's (JCW), grant #MOP-136899 from the Canadian Institutes of Health Research (JCW). Royal Society and ERC Advanced Grant #669237 (DK), Alberta Alzheimer's Research Program award #APRI201700005 (SCF and HW), an Ontario Graduate Scholarship (AL), a scholarship from the Croucher Foundation (RWLS), a Cambridge Trust Scholarship and a Ministry of Education Technologies Incubation Scholarship, Republic of China (Taiwan) (JCS), and by Sidney Sussex College Cambridge (GM).

References

1. Spillantini MG, Goedert M. The alpha-synucleinopathies: Parkinson's disease, dementia with Lewy bodies, and multiple system atrophy. Ann N Y Acad Sci. 2000; 920:16–27. [PubMed: 11193145]
2. Burre J, et al. Alpha-synuclein promotes SNARE-complex assembly in vivo and in vitro. Science. 2010; 329:1663–1667. [PubMed: 20798282]
3. Fujiwara H, et al. alpha-Synuclein is phosphorylated in synucleinopathy lesions. Nat Cell Biol. 2002; 4:160–164. [PubMed: 11813001]
4. Lashuel HA, Overk CR, Oueslati A, Masliah E. The many faces of alpha-synuclein: from structure and toxicity to therapeutic target. Nat Rev Neurosci. 2013; 14:38–48. [PubMed: 23254192]
5. Polymeropoulos MH, et al. Mutation in the α-synuclein gene identified in families with Parkinson's disease. Science. 1997; 276:2045–2047. [PubMed: 9197268]

6. Jucker M, Walker LC. Propagation and spread of pathogenic protein assemblies in neurodegenerative diseases. Nat Neurosci. 2018; 21:1341–1349. [PubMed: 30258241]
7. Scheckel C, Aguzzi A. Prions, prionoids and protein misfolding disorders. Nat Rev Genet. 2018; 19:405–418. [PubMed: 29713012]
8. Mougenot AL, et al. Prion-like acceleration of a synucleinopathy in a transgenic mouse model. Neurobiol Aging. 2012; 33:2225–2228. [PubMed: 21813214]
9. Luk KC, et al. Intracerebral inoculation of pathological alpha-synuclein initiates a rapidly progressive neurodegenerative alpha-synucleinopathy in mice. J Exp Med. 2012; 209:975–986. [PubMed: 22508839]
10. Watts JC, et al. Transmission of multiple system atrophy prions to transgenic mice. Proc Natl Acad Sci U S A. 2013; 110:19555–19560. [PubMed: 24218576]
11. Prusiner SB, et al. Evidence for alpha-synuclein prions causing multiple system atrophy in humans with parkinsonism. Proc Natl Acad Sci U S A. 2015; 112:E5308–5317. [PubMed: 26324905]
12. Luk KC, et al. Pathological alpha-synuclein transmission initiates Parkinson-like neurodegeneration in nontransgenic mice. Science. 2012; 338:949–953. [PubMed: 23161999]
13. Masuda-Suzukake M, et al. Prion-like spreading of pathological alpha-synuclein in brain. Brain. 2013; 136:1128–1138. [PubMed: 23466394]
14. Peng C, Gathagan RJ, Lee VM. Distinct alpha-Synuclein strains and implications for heterogeneity among alpha-Synucleinopathies. Neurobiol Dis. 2018; 109:209–218. [PubMed: 28751258]
15. Alegre-Abarrategui J, et al. Selective vulnerability in alpha-synucleinopathies. Acta Neuropathol. 2019
16. Morales R, Abid K, Soto C. The prion strain phenomenon: molecular basis and unprecedented features. Biochim Biophys Acta. 2007; 1772:681–691. [PubMed: 17254754]
17. Telling GC, et al. Evidence for the conformation of the pathologic isoform of the prion protein enciphering and propagating prion diversity. Science. 1996; 274:2079–2082. [PubMed: 8953038]
18. Guo JL, et al. Distinct α-synuclein strains differentially promote tau inclusions in neurons. Cell. 2013; 154:103–117. [PubMed: 23827677]
19. Bousset L, et al. Structural and functional characterization of two alpha-synuclein strains. Nature communications. 2013; 4
20. Peelaerts W, et al. alpha-Synuclein strains cause distinct synucleinopathies after local and systemic administration. Nature. 2015; 522:340–344. [PubMed: 26061766]
21. Woerman AL, et al. Propagation of prions causing synucleinopathies in cultured cells. Proc Natl Acad Sci U S A. 2015; 112:E4949–4958. [PubMed: 26286986]
22. Peng C, et al. Cellular milieu imparts distinct pathological alpha-synuclein strains in alpha-synucleinopathies. Nature. 2018; 557:558–563. [PubMed: 29743672]
23. Yamasaki TR, et al. Parkinson's disease and multiple system atrophy have distinct alpha-synuclein seed characteristics. J Biol Chem. 2019; 294:1045–1058. [PubMed: 30478174]
24. Candelise N, et al. Seeding variability of different alpha synuclein strains in synucleinopathies. Ann Neurol. 2019; 85:691–703. [PubMed: 30805957]
25. Woerman AL, et al. Multiple system atrophy prions retain strain specificity after serial propagation in two different Tg(SNCA*A53T) mouse lines. Acta Neuropathol. 2019; 137:437–454. [PubMed: 30690664]
26. Giasson BI, et al. Neuronal alpha-synucleinopathy with severe movement disorder in mice expressing A53T human alpha-synuclein. Neuron. 2002; 34:521–533. [PubMed: 12062037]
27. Froula JM, et al. Defining alpha-synuclein species responsible for Parkinson's disease phenotypes in mice. J Biol Chem. 2019; 294:10392–10406. [PubMed: 31142553]
28. Condello C, et al. Structural heterogeneity and intersubject variability of Abeta in familial and sporadic Alzheimer's disease. Proc Natl Acad Sci U S A. 2018; 115:E782–E791. [PubMed: 29311311]
29. Holmes BB, et al. Proteopathic tau seeding predicts tauopathy in vivo. Proc Natl Acad Sci U S A. 2014; 111:E4376–4385. [PubMed: 25261551]
30. Sang JC, et al. Direct Observation of Murine Prion Protein Replication in Vitro. J Am Chem Soc. 2018; 140:14789–14798. [PubMed: 30351023]

31. Aoki N, et al. Atypical multiple system atrophy is a new subtype of frontotemporal lobar degeneration: frontotemporal lobar degeneration associated with alpha-synuclein. Acta Neuropathol. 2015; 130:93–105. [PubMed: 25962793]
32. Herva ME, et al. Anti-amyloid compounds inhibit alpha-synuclein aggregation induced by protein misfolding cyclic amplification (PMCA). J Biol Chem. 2014; 289:11897–11905. [PubMed: 24584936]
33. Hamilton RL. Lewy bodies in Alzheimer's disease: a neuropathological review of 145 cases using alpha-synuclein immunohistochemistry. Brain Pathol. 2000; 10:378–384. [PubMed: 10885656]
34. Heilbronner G, et al. Seeded strain-like transmission of beta-amyloid morphotypes in APP transgenic mice. EMBO Rep. 2013; 14:1017–1022. [PubMed: 23999102]
35. Watts JC, et al. Serial propagation of distinct strains of Abeta prions from Alzheimer's disease patients. Proc Natl Acad Sci U S A. 2014; 111:10323–10328. [PubMed: 24982139]
36. Rasmussen J, et al. Amyloid polymorphisms constitute distinct clouds of conformational variants in different etiological subtypes of Alzheimer's disease. Proc Natl Acad Sci U S A. 2017; 114:13018–13023. [PubMed: 29158413]
37. Sanders DW, et al. Distinct tau prion strains propagate in cells and mice and define different tauopathies. Neuron. 2014; 82:1271–1288. [PubMed: 24857020]
38. Clavaguera F, et al. Brain homogenates from human tauopathies induce tau inclusions in mouse brain. Proc Natl Acad Sci USA. 2013; 110:9535–9540. [PubMed: 23690619]
39. Fares MB, et al. Induction of de novo alpha-synuclein fibrillization in a neuronal model for Parkinson's disease. Proc Natl Acad Sci U S A. 2016; 113:E912–921. [PubMed: 26839406]
40. Holmes BB, et al. Heparan sulfate proteoglycans mediate internalization and propagation of specific proteopathic seeds. Proc Natl Acad Sci U S A. 2013; 110:E3138–3147. [PubMed: 23898162]
41. Mao X, et al. Pathological alpha-synuclein transmission initiated by binding lymphocyte-activation gene 3. Science. 2016; 353
42. Ferreira DG, et al. alpha-synuclein interacts with PrP(C) to induce cognitive impairment through mGluR5 and NMDAR2B. Nat Neurosci. 2017; 20:1569–1579. [PubMed: 28945221]
43. Luna E, et al. Differential alpha-synuclein expression contributes to selective vulnerability of hippocampal neuron subpopulations to fibril-induced toxicity. Acta Neuropathol. 2018; 135:855–875. [PubMed: 29502200]
44. Sorrentino ZA, Giasson BI, Chakrabarty P. alpha-Synuclein and astrocytes: tracing the pathways from homeostasis to neurodegeneration in Lewy body disease. Acta Neuropathol. 2019; 138:1–21. [PubMed: 30798354]
45. Beach TG, et al. Olfactory bulb alpha-synucleinopathy has high specificity and sensitivity for Lewy body disorders. Acta Neuropathol. 2009; 117:169–174. [PubMed: 18982334]
46. Legname G, et al. Continuum of prion protein structures enciphers a multitude of prion isolate-specified phenotypes. Proc Natl Acad Sci USA. 2006; 103:19105–19110. [PubMed: 17142317]
47. Dhillon JS, et al. Comparative analyses of the in vivo induction and transmission of alpha-synuclein pathology in transgenic mice by MSA brain lysate and recombinant alpha-synuclein fibrils. Acta neuropathologica communications. 2019; 7:80. [PubMed: 31109378]
48. Collinge J, Clarke AR. A general model of prion strains and their pathogenicity. Science. 2007; 318:930–936. [PubMed: 17991853]
49. Walsh DM, Selkoe DJ. A critical appraisal of the pathogenic protein spread hypothesis of neurodegeneration. Nat Rev Neurosci. 2016; 17:251–260. [PubMed: 26988744]
50. Surmeier DJ, Obeso JA, Halliday GM. Selective neuronal vulnerability in Parkinson disease. Nat Rev Neurosci. 2017; 18:101–113. [PubMed: 28104909]
51. Chen RH, et al. alpha-Synuclein membrane association is regulated by the Rab3a recycling machinery and presynaptic activity. J Biol Chem. 2013; 288:7438–7449. [PubMed: 23344955]
52. Lee BR, Kamitani T. Improved immunodetection of endogenous α-synuclein. PLoS ONE. 2011; 6:e23939. [PubMed: 21886844]
53. Knowles TP, et al. An analytical solution to the kinetics of breakable filament assembly. Science. 2009; 326:1533–1537. [PubMed: 20007899]

54. Rutherford NJ, Brooks M, Giasson BI. Novel antibodies to phosphorylated alpha-synuclein serine 129 and NFL serine 473 demonstrate the close molecular homology of these epitopes. Acta neuropathologica communications. 2016; 4:80. [PubMed: 27503460]

55. Ip CW, et al. AAV1/2-induced overexpression of A53T-alpha-synuclein in the substantia nigra results in degeneration of the nigrostriatal system with Lewy-like pathology and motor impairment: a new mouse model for Parkinson's disease. Acta neuropathologica communications. 2017; 5:11. [PubMed: 28143577]

Europe PMC Funders Author Manuscripts

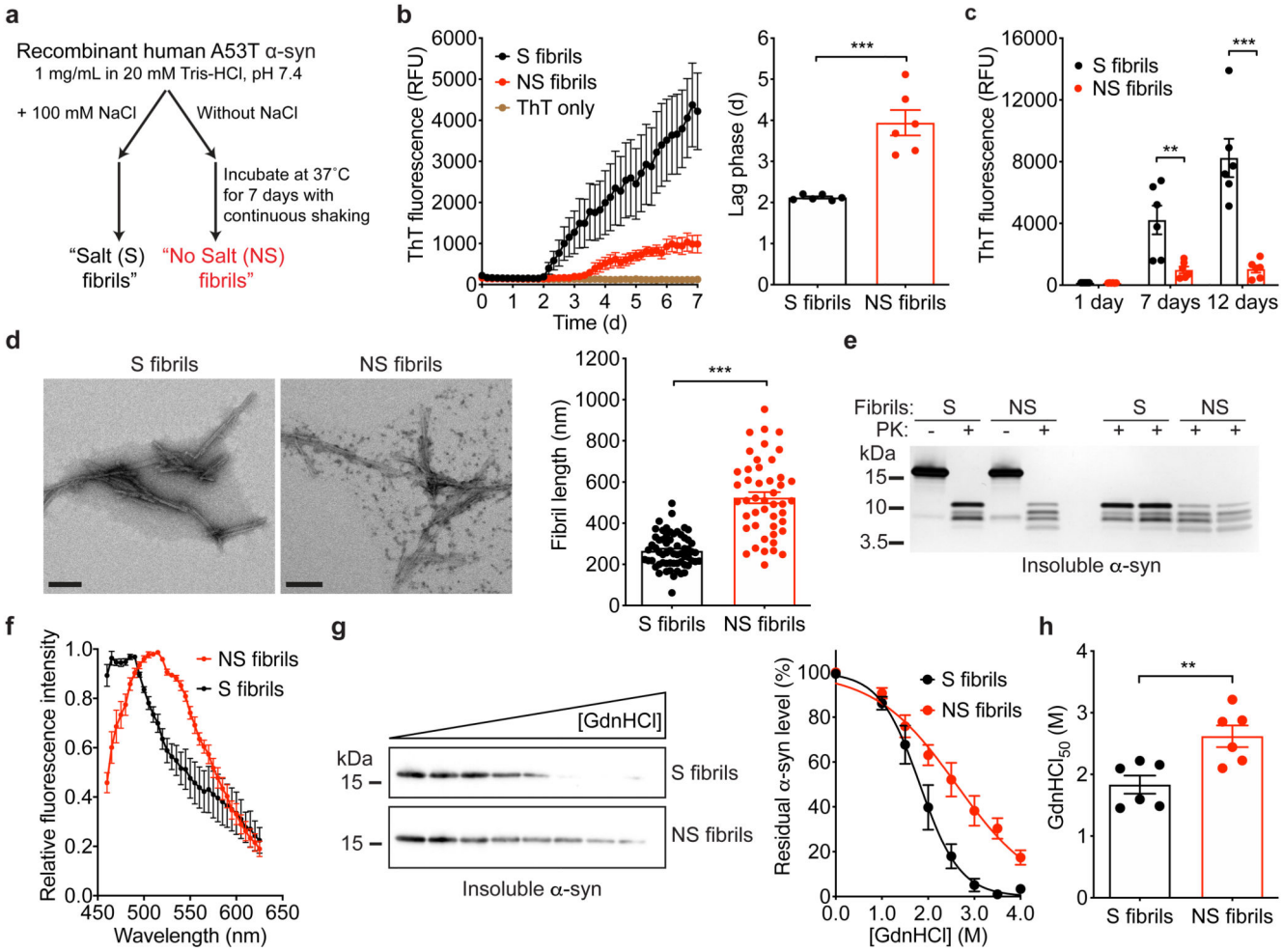

Figure 1. Generation and characterization of recombinant α-syn fibril strains.

a) Conditions used for generating Salt (S) and No Salt (NS) fibrils. **b**) Kinetics of fibril formation for S and NS fibrils in a real-time ThT fluorescence assay. Reactions containing only ThT were used as a negative control. The lag phase for S fibril formation was significantly shorter than the lag phase for NS fibril formation ($P = 1.6 \times 10^{-4}$ by a two-tailed *t*-test). n = 6 biologically independent reactions. Data is mean ± s.e.m. **c**) After either 7 or 12 days of incubation, NS fibrils bind significantly less ThT than S fibrils ($P = 0.0041$ for day 7; $P = 2.7 \times 10^{-8}$ for day 12 by two-way ANOVA with Sidak's multiple comparison test). n = 6 biologically independent reactions. Data is mean ± s.e.m. **d**) At the ultrastructural level, NS fibrils are significantly longer than S fibrils, as determined by electron microscopy ($P = 2.5 \times 10^{-5}$ by a two-tailed *t*-test). n = 3 biologically independent fibril preparations. Data is mean ± s.e.m. Scale bars = 200 nm. **e**) Following digestion with proteinase K (PK), S fibrils and NS fibrils produce different banding patterns of insoluble α-syn species, as assessed by SDS-PAGE followed by silver staining. For both S and NS fibrils, 3 biologically independent fibril preparations were analyzed. **f**) The fluorescence emission spectra for curcumin bound to S and NS fibrils are distinct. Each data point represents the mean relative fluorescence obtained from 3 biologically independent fibril preparations ± s.e.m. **g**)

Europe PMC Funders Author Manuscripts

Conformational stability assay (CSA) for S and NS fibrils. Representative α-syn immunoblots (Syn-1 antibody) and the resultant denaturation curves are shown. The curves depict mean residual α-syn values ± s.e.m. following treatment with the indicated concentrations of GdnHCl. n = 6 biologically independent fibril preparations. **h**) S fibrils are significantly less stable than NS fibrils ($P = 0.0065$ by a two-tailed t-test). n = 6 biologically independent fibril preparations. Data is mean ± s.e.m.

Europe PMC Funders Author Manuscripts

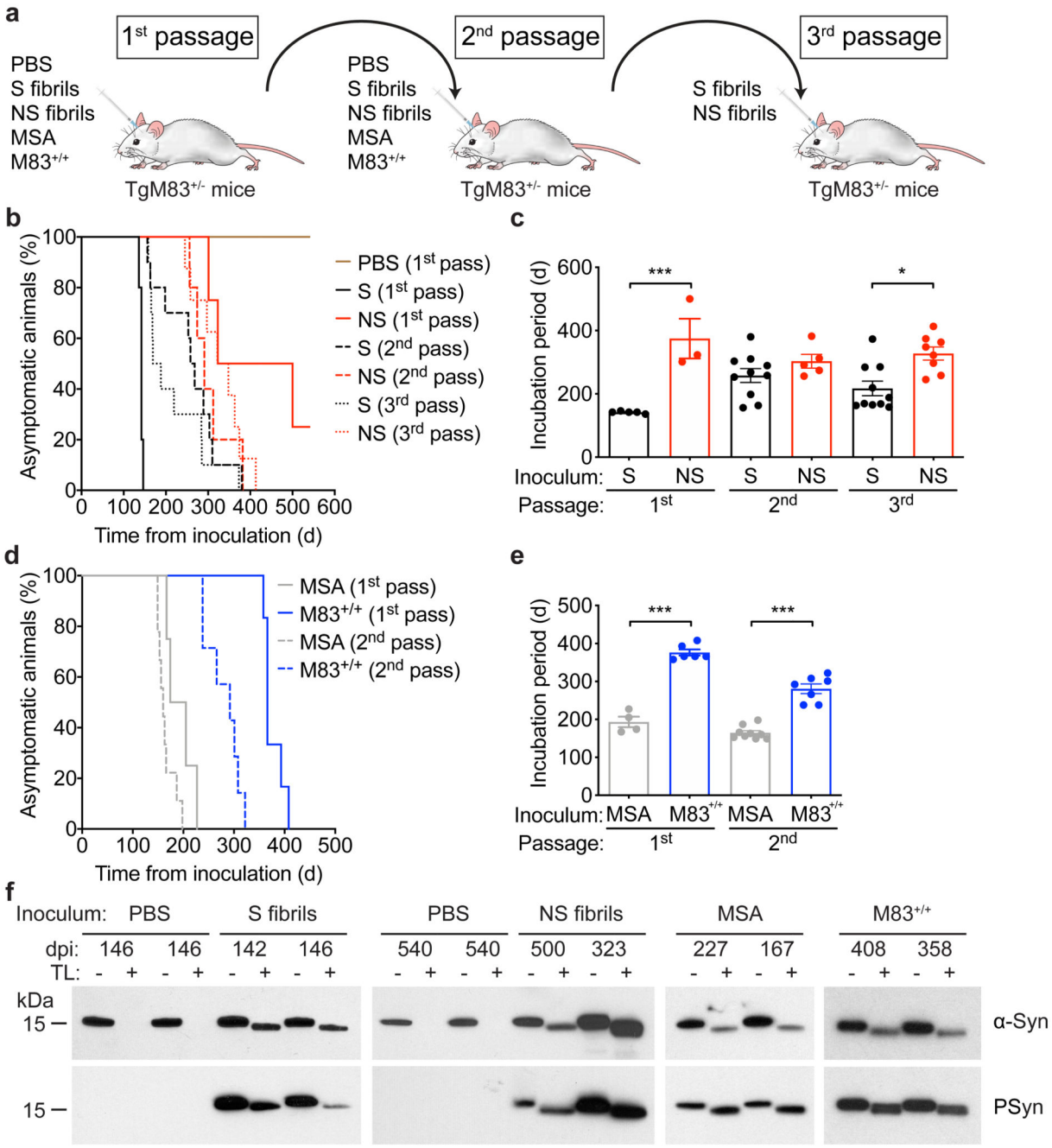

Figure 2. Serial propagation of recombinant and brain-derived α-syn strains in TgM83 mice.

a) Schematic of the serial propagation studies in hemizygous TgM83 mice (TgM83$^{+/-}$). **b**) Kaplan-Meier survival curves for TgM83 mice inoculated with either PBS, S fibrils, or NS fibrils (first, second, or third passage). n = 7 (PBS), 5 (S first passage), 4 (NS first passage), 10 (S second passage), 5 (NS second passage), 10 (S third passage), or 8 mice (NS third passage). **c**) Upon first or third passage, the incubation periods for the NS fibril-derived strain were significantly longer than for the S fibril-derived strain (P = 3.0 x 10^{-4} for first passage; P = 0.013 for third passage by one-way ANOVA with Tukey's multiple

Europe PMC Funders Author Manuscripts

comparisons test). n = 5 (S first passage), 3 (NS first passage), 10 (S second passage), 5 (NS second passage), 10 (S fibrils passage), or 8 mice (NS third passage). Data are mean ± s.e.m. **d**) Kaplan-Meier survival curves for TgM83 mice inoculated with either MSA or $M83^{+/+}$ brain extract (first or second passage). n = 4 (MSA first passage), 6 ($M83^{+/+}$ first passage), 9 (MSA second passage), or 7 mice ($M83^{+/+}$ second passage). **e**) On both first and second passage, the incubation periods for mice injected with the $M83^{+/+}$-derived strain were significantly longer than for mice injected with the MSA-derived strain ($P = 5.6 \times 10^{-10}$ for first passage; $P = 2.5 \times 10^{-8}$ for second passage by one-way ANOVA with Tukey's multiple comparisons test). n = 4 (MSA first passage), 6 ($M83^{+/+}$ first passage), 9 (MSA second passage), or 7 mice ($M83^{+/+}$ second passage). Data are mean ± s.e.m. **f**) Immunoblots of detergent-insoluble α-syn species, with or without thermolysin (TL) digestion, in brain homogenates from asymptomatic PBS-inoculated TgM83 mice or clinically ill TgM83 mice at the indicated days post-inoculation (dpi) with the indicated α-syn strains (first passage). Blots were probed with antibodies to either total α-syn or PSyn. For each inoculum, results from two distinct mice are shown.

Europe PMC Funders Author Manuscripts

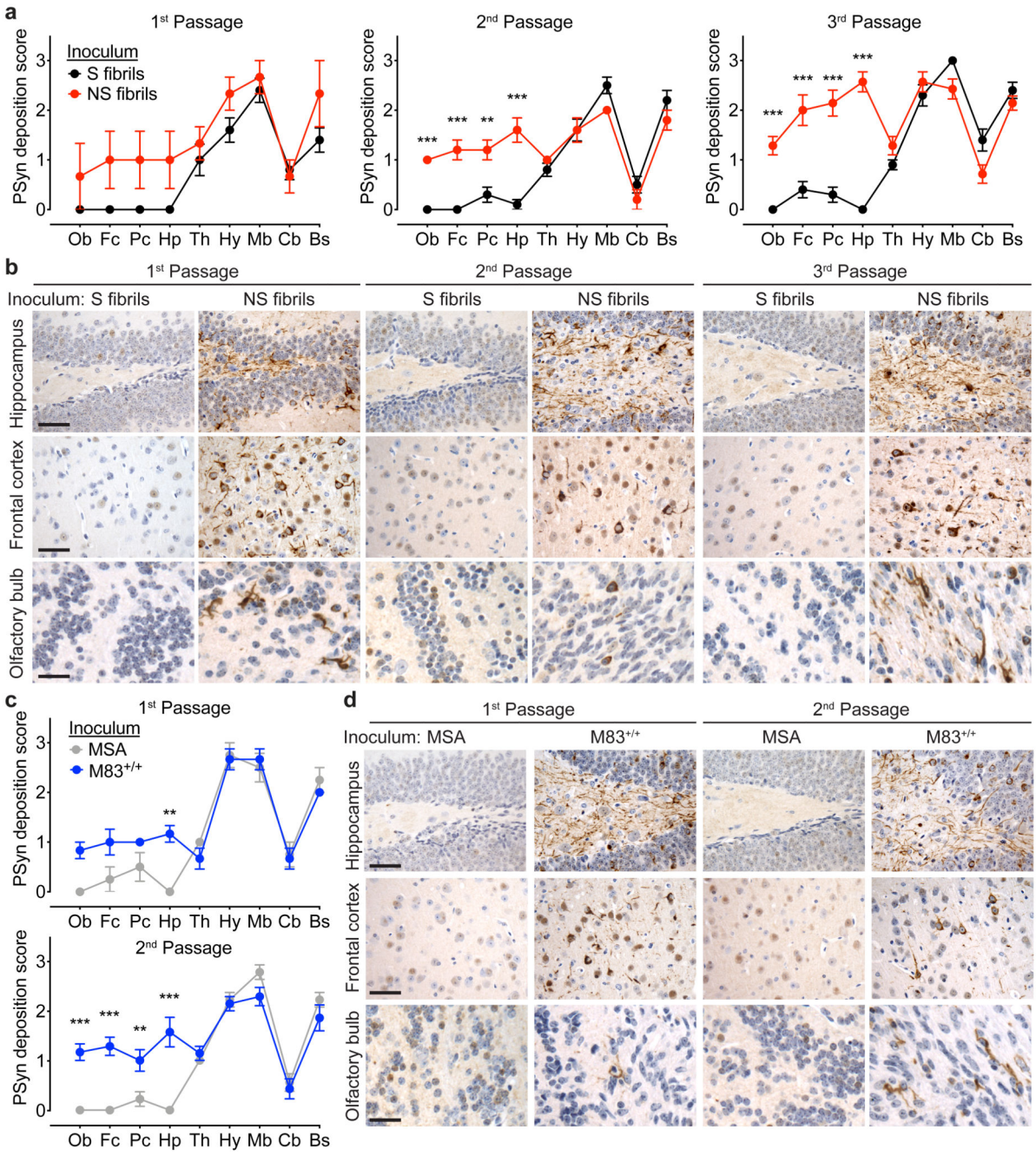

Figure 3. α-Syn strains target distinct brain regions in TgM83 mice.

a) Semiquantitative PSyn deposition scoring within the indicated brain regions from clinically ill TgM83 mice following the first, second, or third passage of the S or NS fibril-derived strains. The patterns of PSyn deposition were significantly different for the S and NS fibril-derived strains upon second ($P = 0.012$) and third passage ($P = 6.5 \times 10^{-5}$), as determined by two-way ANOVA. n = 5 (S first passage), 3 (NS first passage), 10 (S second passage), 5 (NS second passage), 10 (S third passage), or 7 mice (NS third passage). Data are mean ± s.e.m. $^{**}P < 0.01$; $^{***}P < 0.001$ as determined by Sidak's multiple comparisons

test. Ob, olfactory bulb; Fc, frontal cortex; Pc, parietal cortex; Hp, hippocampus; Th, thalamus; Hy, hypothalamus; Mb, midbrain; Cb, cerebellar white matter; Bs, brainstem. **b**) Representative immunohistochemistry images for PSyn in the hippocampus (dentate gyrus region), frontal cortex, or olfactory bulb from mice following inoculation with the S or NS fibril-derived strains (first, second, or third passage). **c**) Semiquantitative PSyn deposition scoring within the indicated brain regions from clinically ill TgM83 mice following the first or second passage of the MSA or $M83^{+/+}$-derived strains. The patterns of PSyn deposition were significantly different for the MSA and $M83^{+/+}$ fibril-derived strains upon second passage ($P = 0.0041$), as determined by two-way ANOVA. n = 4 (MSA first passage), 6 ($M83^{+/+}$ first passage), 9 (MSA second passage), or 7 mice ($M83^{+/+}$ second passage). Data are mean ± s.e.m. $^{**}P < 0.01$; $^{***}P < 0.001$ as determined by Sidak's multiple comparisons test. **d**) Representative immunohistochemistry for PSyn in the hippocampus (dentate gyrus region), frontal cortex, or olfactory bulb from symptomatic mice following inoculation with the MSA or $M83^{+/+}$-derived strains (first or second passage). In b and d, scale bars = 50 μm (hippocampus and frontal cortex) or 25 μm (olfactory bulb).

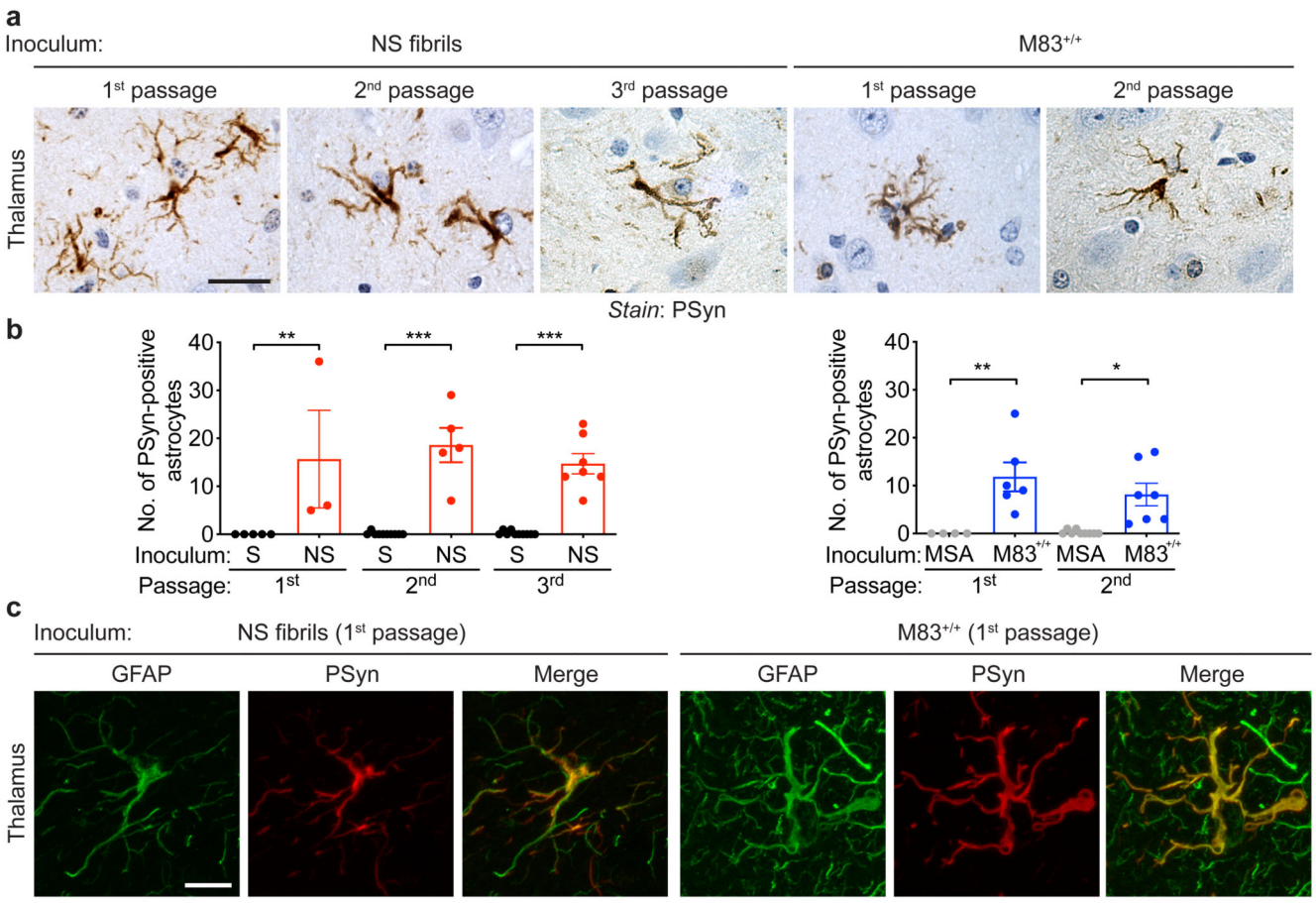

Figure 4. The NS fibril and M83$^{+/+}$-derived α-syn strains selectively target astrocytes in TgM83 mice.

a) Representative immunohistochemistry images for PSyn in the thalamus of clinically ill TgM83 mice inoculated with either the NS fibril-derived strain (first, second, or third passage) or the M83$^{+/+}$-derived strain (first or second passage) reveals α-syn pathology within astrocytes. Scale bar = 25 μm (applies to all images). **b**) Quantification of PSyn-positive astrocytes within the thalamus of TgM83 mice inoculated with either the S or NS fibril-derived strains (first, second, or third passage) as well as all TgM83 mice inoculated with either the MSA- or M83$^{+/+}$-derived strains (first or second passage). Significantly more PSyn-positive astrocytes were present in mice inoculated with the NS fibril-derived strain compared to mice inoculated with the S fibril-derived strain (P = 0.0064, 1.1 x 10^{-5}, and 1.1 x 10^{-4} for first, second, and third passages, respectively) as well as in mice inoculated with the M83$^{+/+}$-derived strain compared to mice inoculated with the MSA-derived strain (P = 0.0047 and 0.016 for first and second passages, respectively), as determined by one-way ANOVA with Tukey's multiple comparisons test. n = 5 (S first passage), 3 (NS first passage), 10 (S second passage), 5 (NS second passage), 10 (S third passage), 7 (NS third passage), 4 (MSA first passage), 6 (M83$^{+/+}$ first passage), 9 (MSA second passage), or 7 mice (M83$^{+/+}$ second passage). Data are mean ± s.e.m. **c**) Co-localization of PSyn (red) and glial fibrillary acidic protein (GFAP; green) staining in double-labeled sections of the

thalamus from TgM83 mice inoculated with either NS fibrils or $M83^{+/+}$ brain extract (first passage). Scale bar = 10 μm (applies to all images).

Europe PMC Funders Author Manuscripts

Europe PMC Funders Author Manuscripts

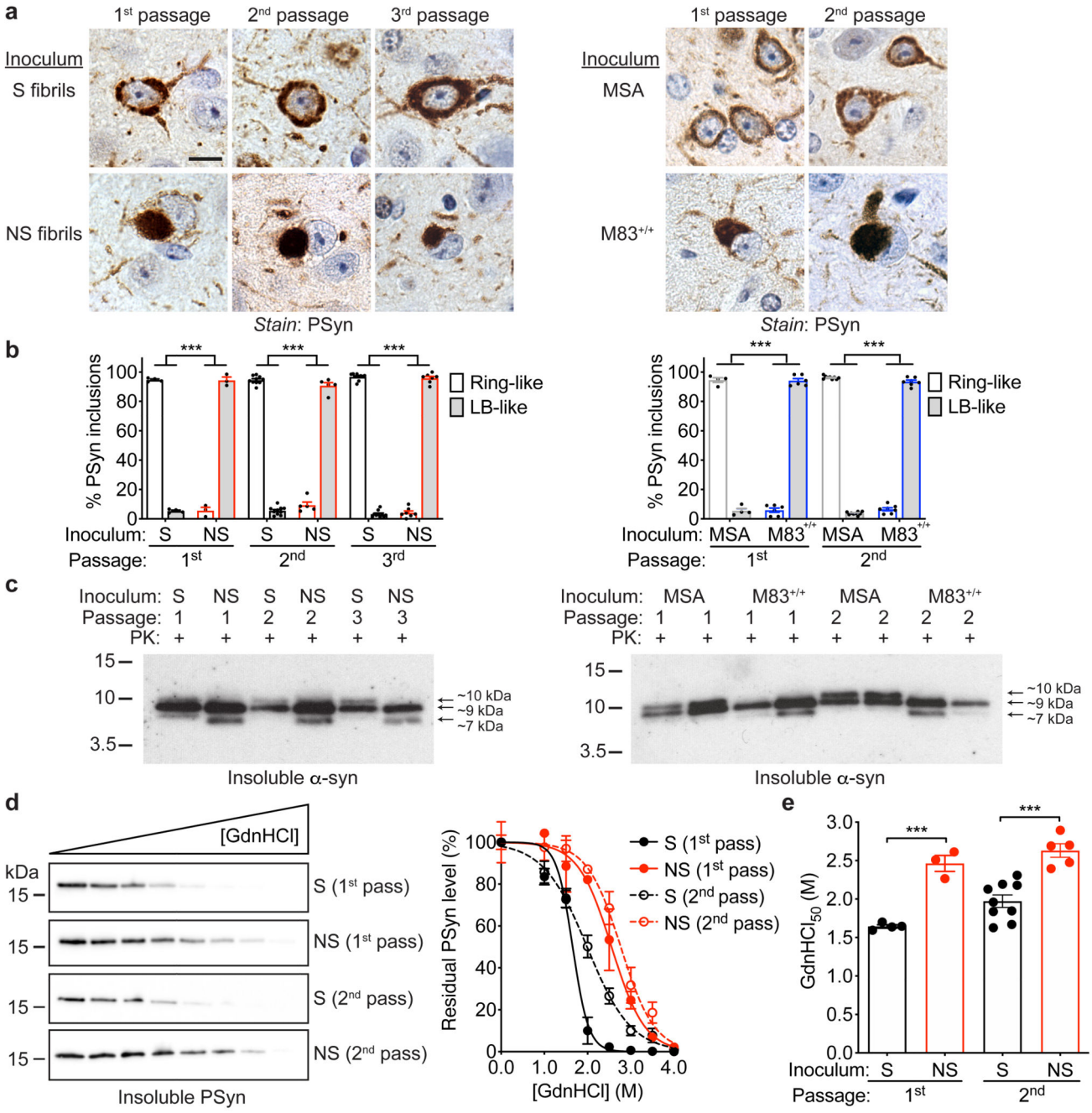

Figure 5. Conformational discrimination of α-syn strains in the brains of inoculated TgM83 mice.

a) Representative immunohistochemistry images for PSyn in the midbrain of clinically ill TgM83 mice inoculated with either the S or NS fibril-derived strains (first, second, or third passage), or with the MSA or M83$^{+/+}$-derived strains (first or second passage). Neurons in mice inoculated with the S or MSA strains contain “ring-like” PSyn deposits whereas neurons in mice inoculated with the NS or M83$^{+/+}$ strains contain “LB-like” PSyn deposits. Scale bar = 10 μm (applies to all images). **b**) Quantification of ring-like vs. LB-like PSyn

inclusions in the midbrain of inoculated TgM83 mice. The distribution of PSyn inclusions was significantly different in mice inoculated with the NS fibril-derived strain compared to mice inoculated with the S fibril-derived strain ($P = 5.5 \times 10^{-14}$) as well as in mice inoculated with the $M83^{+/+}$-derived strain compared to mice inoculated with the MSA-derived strain ($P = 2.3 \times 10^{-14}$), as determined by one-way ANOVA with Tukey's multiple comparisons test. n = 5 (S ffirst passage), 3 (NS first passage), 10 (S second passage), 5 (NS second passage), 10 (S third passage), 7 (NS third passage), 4 (MSA first passage), 6 ($M83^{+/+}$ first passage), 9 (MSA second passage), or 7 mice ($M83^{+/+}$ second passage). Data are mean ± s.e.m. **c**) Immunoblots of detergent-insoluble α-syn species in brain homogenates from inoculated TgM83 mice following treatment with PK. Blots were probed with the Syn-1 antibody. **d**) CSA for PSyn aggregates from all TgM83 mice inoculated with either the S or NS fibril-derived strains (first or second passage). Representative PSyn immunoblots and the resultant denaturation curves are shown. The curves depict mean residual PSyn values ± s.e.m. following treatment with the indicated concentrations of GdnHCl. **e**) The $GdnHCl_{50}$ values for PSyn aggregates in mice inoculated with the S fibril-derived strain are significantly lower than in mice injected with the NS fibril-derived strain ($P = 3.3 \times 10^{-4}$ for first passage and $P = 1.1 \times 10^{-4}$ for second passage, as determined by one-way ANOVA with Tukey's multiple comparisons test). Data are mean ± s.e.m. For d and e, n = 4 (S first passage), 3 (NS first passage), 9 (S second passage), or 5 mice (NS second passage).

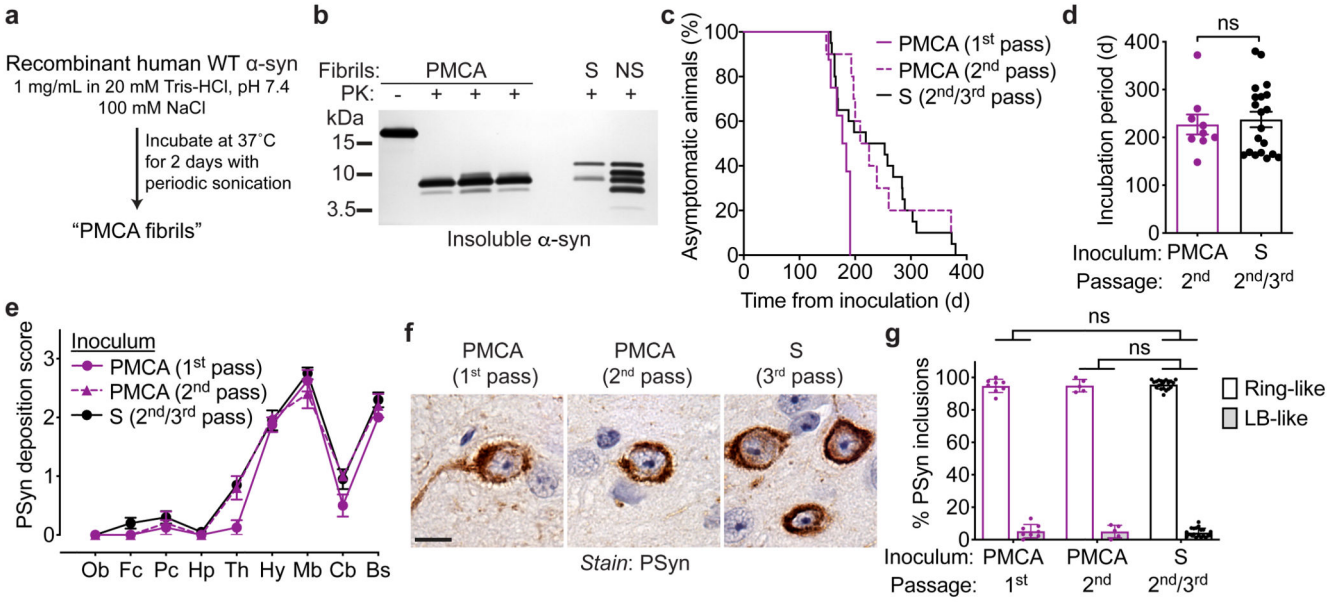

Figure 6. PMCA-generated α-syn fibrils produce a phenotype similar to that induced by S fibrils upon propagation in TgM83 mice.

a) Conditions used for generating PMCA α-syn fibrils. **b**) Following digestion with PK, PMCA fibrils exhibit a different banding pattern of insoluble α-syn species than either S or NS fibrils, as assessed by SDS-PAGE followed by silver staining. Results from three independent preparations of PMCA fibrils are shown. **c**) Kaplan-Meier survival curves for TgM83 mice inoculated with the PMCA fibril-derived strain (first or second passage) or the S fibril-derived strain (pooled data from second and third passages). n = 8 (PMCA first passage), 10 (PMCA second passage) or 20 mice (S second/third passages). **d**) Upon second passage, the incubation periods obtained with the PMCA-derived strain were similar to those for the S fibril-derived strain (pooled data from second and third passages). n = 9 (PMCA second passage) or 20 mice (S second/third passages). Data are mean ± s.e.m. ns, not significant ($P = 0.71$ by a two-tailed t-test). **e**) Semiquantitative PSyn deposition scoring (data are mean ± s.e.m.) within the indicated brain regions from clinically ill TgM83 mice following inoculation with the PMCA fibril-derived strain (first or second passage, n = 8 or 5, respectively) or the S fibril-derived strain (pooled data from second and third passages, n = 20). The patterns of PSyn deposition are not significantly different between the three groups ($P = 0.063$ by two-way ANOVA). **f**) Representative immunohistochemistry images for PSyn in the midbrain of TgM83 mice inoculated with either the PMCA fibril-derived strain (first or second passage) or the S fibril-derived strain (third passage). The PMCA fibril-derived strain exhibits "ring-like" PSyn inclusions similar to those present in mice injected with the S fibril-derived strain. Scale bar = 10 μm (applies to all images). **g**) Quantification of ring-like vs. LB-like PSyn inclusions in the midbrain of TgM83 mice inoculated with the PMCA fibril-derived strain (n = 8 for first passage, n = 5 for second passage) compared to mice inoculated with the S fibril-derived strain (pooled data from second and third passages, n = 20). There was no difference in the distribution of ring-like vs. LB-like PSyn inclusions between either the first ($P = 0.80$) or second ($P = 0.91$) passages

of the PMCA fibril-derived strain and the S fibril-derived strain, as determined by one-way ANOVA with Tukey's multiple comparisons test. Data are mean ± s.e.m.

Europe PMC Funders Author Manuscripts

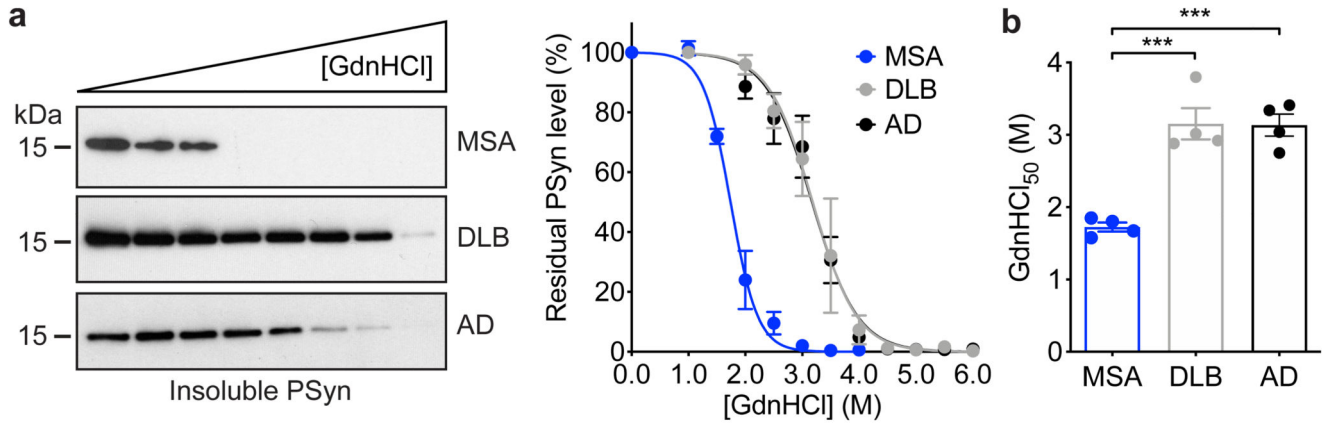

Figure 7. Conformational discrimination of α-syn strains in human synucleinopathies.

a) CSA for PSyn aggregates in brain extracts from patients with MSA, DLB, or AD with concomitant PSyn deposition. Representative PSyn immunoblots and the resultant denaturation curves are shown. The curves depict mean residual PSyn values ± s.e.m. following treatment with the indicated concentrations of GdnHCl. For each disease, samples from four different patients were analyzed. **b**) Significantly higher $GdnHCl_{50}$ values were obtained for PSyn aggregates in DLB ($P = 3.2 \times 10^{-4}$) and AD patients ($P = 3.5 \times 10^{-4}$) than for MSA patients (n = 4 each), as determined by one-way ANOVA with Tukey's multiple comparisons test. Data are mean ± s.e.m.

Europe PMC Funders Author Manuscripts

Europe PMC Funders Author Manuscripts

Table 1
Disease incubation periods for inoculated TgM83 mice

Inoculum	α-Syn sequence in inoculum	1st passage		2nd passage[1]		3rd passage[1]	
		Mean incubation time ± s.e.m. (d)	n/n_0[2]	Mean incubation time ± s.e.m. (d)	n/n_0	Mean incubation time ± s.e.m. (d)	n/n_0
None	NA[3]	> 540[4]	0/13	ND[3]		ND	
PBS	NA	> 540	0/7	> 400	0/9	ND	
α-Syn monomers	WT	> 362	0/8	ND		ND	
	A53T	> 541	0/7	ND		ND	
S fibrils	A53T	142 ± 2	5/5	258 ± 22	10/10	217 ± 23	10/10
NS fibrils	A53T	375 ± 63	3/4[5]	303 ± 22	5/5	328 ± 21	8/8
PMCA fibrils	WT	176 ± 6	8/8	227 ± 21	9/10[6]	ND	
$M83^{+/+}$	A53T	376 ± 8	6/6	281 ± 13	7/7	ND	
MSA	WT	193 ± 14	4/4	165 ± 6	9/9	ND	
DLB	WT	> 540	0/5	ND		ND	
AD	WT	> 540	0/4	ND		ND	

[1] for the 2nd passage, mice were inoculated with brain homogenate from 1st passage mice previously inoculated with the indicated inoculum; for the 3rd passage, mice were inoculated with brain homogenate from 2nd passage mice.

[2] n, number of mice with neurological dysfunction and cerebral PSyn deposition; n_0, number of mice observed; does not include mice that died of intercurrent illness (see Supplementary Table 4).

[3] NA, not applicable; ND, not determined.

[4] mice were examined up until 580 days of age, which corresponds to ~540 days following mock inoculation.

[5] one mouse remained healthy at 540 dpi

[6] one mouse remained healthy at 375 dpi